

---

# Tactile MNIST: Benchmarking Active Tactile Perception

---

Tim Schneider<sup>1,2</sup>, Guillaume Duret<sup>2</sup>, Cristiana de Farias<sup>1</sup>,  
Roberto Calandra<sup>3</sup>, Liming Chen<sup>2</sup>, and Jan Peters<sup>4</sup>

<sup>1</sup> Department of Computer Science, TU Darmstadt, Germany.

<sup>2</sup> LIRIS, CNRS UMR5205, Ecole Centrale de Lyon, France.

<sup>3</sup> LASR Lab & CeTI, TU Dresden, Germany.

<sup>4</sup> DFKI, Hessian.AI, and Centre for Cognitive Science, TU Darmstadt, Germany.

## Abstract

Tactile perception has the potential to significantly enhance dexterous robotic manipulation by providing rich local information that can complement or substitute for other sensory modalities such as vision. However, because tactile sensing is inherently local, it is not well-suited for tasks that require broad spatial awareness or global scene understanding on its own. A human-inspired strategy to address this issue is to consider active perception techniques instead. That is, to actively guide sensors toward regions with more informative or significant features and integrate such information over time in order to understand a scene or complete a task. Both active perception and different methods for tactile sensing have received significant attention recently. Yet, despite advancements, both fields lack standardized benchmarks. To bridge this gap, we introduce the *Tactile MNIST Benchmark Suite*, an open-source, Gymnasium-compatible benchmark specifically designed for active tactile perception tasks, including localization, classification, and volume estimation. Our benchmark suite offers diverse simulation scenarios, from simple toy environments all the way to complex tactile perception tasks using vision-based tactile sensors. Furthermore, we also offer a comprehensive dataset comprising 13,500 synthetic 3D MNIST digit models and 153,600 real-world tactile samples collected from 600 3D printed digits. Using this dataset, we train a CycleGAN for realistic tactile simulation rendering. By providing standardized protocols and reproducible evaluation frameworks, our benchmark suite facilitates systematic progress in the fields of tactile sensing and active perception.

**Project page:** <https://sites.google.com/robot-learning.de/tactile-mnist>

## 1 Introduction

Tactile perception is fundamental for enabling agents to interact effectively with their environments. Studies of humans with impaired touch reveal that they face significant challenges in grasping and performing routine manipulation tasks due to insufficient feedback about contact states between fingers and objects [4]. Moreover, touch often complements—or even substitutes—other sensory modalities such as vision: we feel the shape of a hard-to-see object on a high shelf, count cookies in a jar without looking, or locate a key inside a bag purely by touch. Unlike vision, which typically offers a broad field of view, touch provides highly localized yet information-rich feedback confined to the point of contact [5, 6]. It is this inherently interactive nature that enables agents (such as robots) to explore visually occluded areas, classify textures, infer material properties like stiffness

---

Corresponding Author: [tim@robot-learning.de](mailto:tim@robot-learning.de)

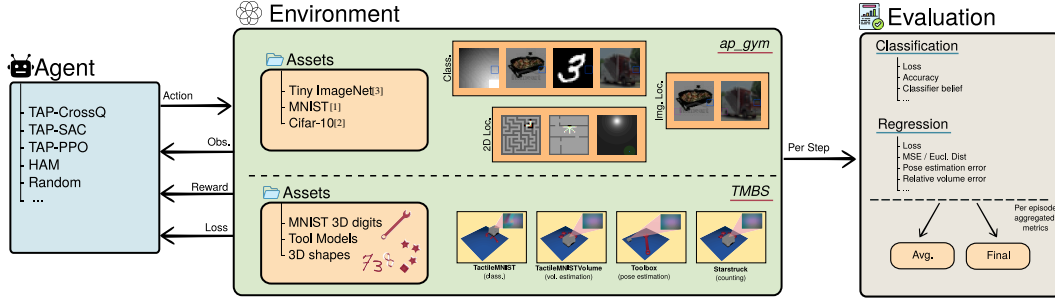


Figure 1: Overview of the *Active Perception Gym* (ap\_gym), the *Tactile MNIST Benchmark Suite* (TMBS), and their associated assets. In the center we depict each environment from ap\_gym and TMBS, along with the included asset sets (both custom and external). On the left, an agent (e.g., an active perception algorithm) interacts with the environment by receiving observations, rewards, and losses, and returning actions. On the right, we show task-specific evaluation metrics, available at each step, with support for both per-step outputs and aggregated performance scores.

and friction, and detect fine local features of objects [7, 8, 9, 10, 11, 12, 13, 14]. However, without standardized benchmarks and widely adopted datasets, it becomes difficult to rigorously evaluate new algorithms, reproduce results, or compare different approaches in a fair way. Yet, despite its growing importance, the field of tactile sensing still lacks such structured benchmarks and community-wide datasets tailored to touch-related tasks

In contrast to tactile sensing, computer vision has significantly benefited from such standardized datasets and clearly defined evaluation protocols. MNIST [1] established an early baseline for digit recognition that is still relevant today. Datasets such as ImageNet [15] and COCO [16] expanded both scale and complexity, driving major advances in object classification, detection, and scene understanding. Additionally, domain-specific benchmarks such as KITTI [17] and Omni3D [18] have enabled focused progress on challenges like fine-grained categorization and robustness in real-world applications. By comparison, the few tactile perception benchmarks in the literature still rely on custom hardware or narrowly scoped datasets, which limits their generalizability and slows broader adoption [14, 19].

In this work, we focus explicitly on benchmarking *active tactile perception* tasks where agents deliberately interact with their environment to gather task-relevant information. Active perception involves strategic decisions about where and when to sense, efficiently choosing actions that maximize information gain [10, 9, 20, 8]. Here, as each contact takes time, resources, and may cause wear on sensors or environments, efficiency becomes a central concern: agents must extract as much information as possible using as few interactions as necessary. A well-designed benchmark for active tactile perception can help answer key questions such as: How should an agent select contact points to maximize information gain? What policies enable accurate inference with minimal touch? How does uncertainty (from sensor noise, ambiguous contact, or environmental variability) affect the trade-off between exploration and confidence?

We introduce *Active Perception Gym* (ap\_gym)<sup>1</sup>, a framework compatible with Gymnasium [21], designed to benchmark active perception algorithms. ap\_gym includes nine toy scenarios where an agent must learn to efficiently extract information to solve perception tasks. Building on ap\_gym, we present the *Tactile MNIST Benchmark Suite* (TMBS)<sup>2</sup>, which extends the framework to simulated active tactile perception problems. In TMBS, agents control a simulated GelSight Mini sensor [22] without access to visual inputs. Tactile perception tasks include MNIST-style classification of 3D digit models, pose estimation of tools on platforms, and object counting. Across all tasks, the agent must actively determine *what* to sense and strategically select *where and when* to explore through touch. Thus, solving these tasks requires solving a dual problem: making accurate predictions from past observations while optimizing an exploration policy to maximize information gain. An overall visualization of our framework and tasks in ap\_gym and TMBS is shown in Fig. 1.

<sup>1</sup><https://github.com/TimSchneider42/active-perception-gym>

<sup>2</sup><https://github.com/TimSchneider42/tactile-mnist>

Table 1: Comparison of Active Tactile Perception Benchmarks. Tactile modalities are **bolded**.

Method	Dataset Available	Active Benchmark	Sensor Modality
Active Vision Grasp [24]	✗	✓	Vis
R3ED [25]	✓	✓	Vis
Robotic Vision Challenge [26]	✗	✓	Vis
NBV_Bench [27]	✓	✓	Vis
AVD [28, 29]	✓	✓	Vis
Active Object Search [30]	✓	✓	Vis
ActiView [31]	✓	✓	Vis+Text
TIP Bench. [32]	✗	✗	<b>Tac</b>
FoTa [33]	✓	✗	<b>Tac</b>
YCB-Slide [34]	✓	✗	<b>Tac</b>
TacBench [14]	✓	✗	<b>Tac</b>
ActiveCloth [35]	✓	✗	<b>Tac</b>
Touch and Go [36]	✓	✗	<b>Tac+Vis</b>
FeelSight [19]	✓	✗	<b>Tac+Vis</b>
ViTac [37]	✗	✗	<b>Tac+Vis</b>
SSVTP [13]	✓	✗	<b>Tac+Vis</b>
GelFabric [38]	✓	✗	<b>Tac+Vis</b>
VisGel [39]	✓	✗	<b>Tac+Vis</b>
PHYSICLEAR [40]	✓	✗	<b>Tac+Text</b>
TVL [41]	✓	✗	<b>Tac+Vis+Text</b>
Touch100k [42]	✓	✗	<b>Tac+Vis+Text</b>
ObjectFolder [43, 44, 45]	✓	✗	<b>Tac+Vis+Audio</b>
<b>Ours</b>	✓	✓	<b>Tac</b>

With this benchmark, our goal is to provide a reproducible and accessible evaluation framework for the tactile perception community. To that end, TMBS is a fully *simulated* environment that is easy to set up and enables rapid, consistent comparisons, without the need to replicate a complex real-world setup. However, we acknowledge the inherent challenges and noise present in real-world tactile data that are often absent in simulation. To help bridge this sim-to-real gap, we complement our simulated environment with a large-scale dataset of 13,580 high-fidelity 3D object models. From this collection, we 3D-printed 600 objects and constructed a curated real-world dataset comprising 153,600 tactile contacts, each annotated with detailed temporal and spatial metadata. We further leverage this dataset to train a CycleGAN [23], enabling the rendering of realistic tactile signals within the simulation.

In summary, our main contributions are:

- To the best of our knowledge, we introduce the first benchmark suite specifically for active *tactile* perception. It offers a range of tasks from simple toy problems to challenging, high-dimensional scenarios.
- We further introduce `ap_gym`, an extensible framework for generic active perception algorithms. `ap_gym` is Gymnasium compatible and is, thus, easy to integrate with existing reinforcement-learning pipelines, enabling fair evaluation.
- We provide an open dataset of 13,580 high-resolution 3D models of handwritten digits, designed for both simulated tactile-image generation and physical 3D printing.
- From our library of 3D models, we 3D-printed 600 objects and captured 153,600 tactile contacts using a GelSight Mini sensor, each annotated with spatial location and class labels.

## 2 Related Work

**(Active) Tactile Perception:** Tactile sensing enables robots to infer object geometry, texture and material properties through physical contact, complementing or, in some cases, substituting vision. Vision-based tactile sensors such as GelSight [22] and DIGIT [46] have become widely available, producing high-resolution “tactile images” that capture local surface features and force distributions. These rich signals have been exploited for shape reconstruction and material recognition [7, 32, 41, 40], as well as advanced dexterous manipulation [47, 48, 19].

Much of the work in tactile sensing, however, focuses on passive touch: the robot either registers a single contact or follows a predefined exploration policy. Inspired by the successes of active vision (as well as by early research on active touch in robotics [49, 50]), recent efforts have revisited the idea of tactile exploration as an active, decision-driven process. In this framing, the robot dynamically

selects where and how to touch next, rather than relying on a fixed sequence of actions. Gaussian process and Bayesian optimization have been employed to drive this active exploration, yielding significant improvements in tasks such as shape reconstruction, texture classification and grasp planning [10, 7, 51]. Reinforcement-learning based approaches [9] tackle active exploration in high-dimensional tactile state spaces. Furthermore, [8] introduced HAM a selective-attention mechanism to optimize scene exploration, and in [52] task-agnostic strategies generalize active touch across different objectives. Additionally, [35] demonstrated how Kinect-based vision can guide active touch for material classification, and [13] proposed a self-supervised visuo-tactile pretraining scheme that benefits both passive and active perception tasks.

**Benchmarking Methods for Tactile Sensing & Active Perception:** Over the past decade, the active vision community has produced a number of datasets and challenges to evaluate a range of tasks. Early work such as the Active Vision Dataset (AVD) provided large-scale Kinect captures for navigation and class-incremental learning tasks [28, 29]. Subsequent efforts explored next-best-view planning for classification (NBV\_Bench [27]), heuristic and data-driven view selection for grasp synthesis on YCB objects [24], and embodied 3D exploration in real indoor scenes (R3ED [25]). Simulation-based approaches such as the Robotic Vision Scene Understanding Challenge [26] and Active Object Search [30] have further expanded evaluation protocols for semantic SLAM and object detection tasks. More recently, multi-modal active perception has been addressed by ActiView, which tests an agent’s ability to zoom and pan to answer vision-language queries [31].

In parallel, tactile sensing research has released a diverse set of characterization benchmarks (TIP Bench. [32]), texture and material recognition datasets (ActiveCloth [35], ViTac [37], SSVTP [13], GelFabric [38]), and cross-modal vision–touch benchmarks and datasets (VisGel [39], Touch and Go [36], PHYSICLEAR [40], FeelSight [19], TacBench [14]). Large-scale multimodal datasets such as Touch100k [42], TVL [41], and FoTa [33] now exceed tens of thousands of samples across vision, touch, and language modalities. Multisensory datasets like ObjectFolder [43, 44, 53] further integrate tactile, visual, and audio data. In a similar manner, efforts to standardize vision-based tactile simulation have led to platforms like TACTO [54] and Taxim [55], which enable high-resolution visuo-tactile data generation. Despite these efforts, only the datasets provided by ActiveCloth [35] and SSVTP [13] support downstream active tactile perception tasks. However, these works do not provide standardized evaluation protocols or benchmarks to systematically evaluate active perception approaches. A comparison of existing datasets and benchmarks is summarized in Table 1. To the best of our knowledge, our proposed Tactile MNIST Benchmark Suite is the first to introduce a dedicated and reproducible benchmark for *active tactile perception*, where tactile exploration is an integral component of the perceptual process.

### 3 Framework: Benchmarking Active Perception

In this section, we introduce both the *Active Perception Gym* (ap\_gym), a framework for benchmarking active perception algorithms, and the *Tactile MNIST Benchmark Suite* (TMBS), which introduces environments for four active tactile perception tasks. Fig. 1 depicts an overview of our framework.

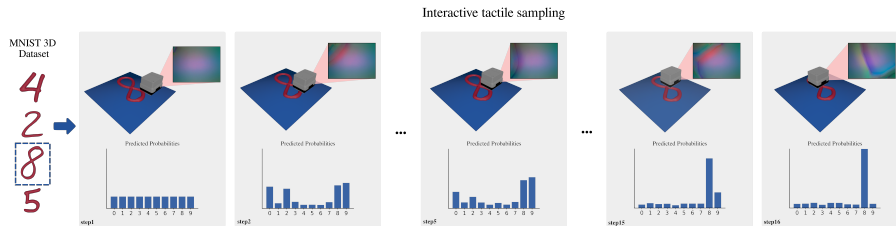


Figure 2: Illustration of the TactileMNIST classification task. In each episode of the TactileMNIST classification task, one random digit from the MNIST 3D dataset is selected and presented to the agent. It can then move the sensor around and touch the object 16 times before the episode terminates. Notably, it does not receive any visual input but has to rely solely on the readings from its tactile sensor. After every touch, it has to make a prediction about the class label, the digit’s numeric value, and its performance is measured by the average prediction accuracy throughout the episode.



Table 2: Overview of the environments, including task types, descriptions, and assets.

Suite	Environment	Task Type	Description	Assets
ap_gym	TinyImageNet	Classification	Classify natural images into 200 categories by moving a limited field-of-view glimpse.	Tiny ImageNet [3]
	CIFAR10	Classification	Classify natural images into 10 categories by moving a limited field-of-view glimpse.	CIFAR-10 [2]
	CircleSquare	Classification	Determine whether a given image contains a circle or a square using limited agent visibility.	Geometric shapes
	MNIST	Classification	Digit recognition task using standard MNIST digits.	MNIST [1]
	LightDark	Regression (2D localization)	Position estimation from brightness-dependent noisy observations, requiring movement to light.	None
	LIDARLocRooms	Regression (2D localization)	Navigate procedurally generated maps with ambiguous LIDAR readings to localize.	None
	LIDARLocMaze	Regression (2D localization)	Navigate procedurally generated mazes with ambiguous LIDAR readings to localize.	None
	TinyImageNetLoc	Regression (2D patch localization)	Localize a glimpse within a natural image by moving a limited field-of-view.	Tiny ImageNet [3]
TMBS	CIFAR10Loc	Regression (2D patch localization)	Localize a glimpse within a natural image by moving a limited field-of-view.	CIFAR-10 [2]
	TactileMNIST	Classification	Touch-based digit classification using a vision-based tactile sensor.	MNIST 3D digits
	TactileMNISTVolume	Regression (volume estimation)	Estimate volume of digits using a vision-based tactile sensor.	MNIST 3D digits
	Toolbox	Regression (object pose estimation)	Estimate 6D pose of tools (e.g., a wrench) using a vision-based tactile sensor.	3D tools
	Starstruck	Classification (counting)	Count stars among other objects using a vision-based tactile sensor.	3D shapes

### 3.1 Active Perception

In active perception tasks, an agent’s main objective is to gather information and make predictions about a desired property of the environment, e.g., the class label or pose of an object. Examples of such properties could be the location of an object in case of a search task or the class of an object for the agent in case of a classification task. To gather information, the agent must interact with the environment, e.g., by moving a sensor around a platform in case of TMBS.

We model active perception as an episodic process, where the agent can take a number of time-discrete sequential actions until the episode terminates and is reset. At every step, the agent obtains an observation (e.g., a tactile glimpse) from the environment that reveals some information but never the full state at once. Formally, that makes active perception problems a special case of Partially Observable Markov Decision Processes (POMDPs).

POMDPs are defined by the tuple  $(S, A, T, R, \Omega, O, \gamma)$ , consisting hidden states  $S$ , actions  $A$ , a transition function  $T : S \times A \times S \rightarrow [0, 1]$ , a reward function  $R : S \times A \rightarrow \mathbb{R}$ , a set of observations  $\Omega$ , an observation function  $O : S \times A \times \Omega \rightarrow [0, 1]$ , and a discount factor  $\gamma \in [0, 1]$ . The objective of the agent in a POMDP is to maximize the expected cumulative reward over time by selecting actions based on its belief about the underlying state. Since the agent does not have direct access to the true state, it maintains a belief distribution over states, updating it using observations and the observation function. The environment evolves according to the transition function, where taking an action leads to a probabilistic transition to a new state, which in turn generates an observation based on the observation function.

In case of active perception problems, we assume that the hidden state  $S$ , the action  $A$ , the reward function  $R$ , and the transition function  $T$  have specific structures. First, we assume that the target property the agent is tasked to predict is part of the hidden state. Hence,  $S$  is defined as  $S = S_{\text{base}} \times Y^*$ , where  $S_{\text{base}}$  is the set of base (hidden) states of the environment and  $Y^*$  is the set of prediction targets. E.g.,  $Y^*$  could be the set of classes in a classification task or the set of possible locations in a localization task, while  $S_{\text{base}}$  contains all the other hidden state information. To allow the agent to make predictions, the action space  $A$  is defined as  $A_{\text{base}} \times Y$ , where  $A_{\text{base}}$  is the base action space and  $Y$  is the prediction space. The base action space  $A_{\text{base}}$  contains all the actions the agent can take to interact with the environment, while  $Y$  is the set of possible predictions the agent can make. Crucially, environments are defined in a way that the agent’s prediction never influences the hidden state of the environment. Thus, the transition function  $T$  is defined as  $T(s, a, s') = T(s, (a_{\text{base}}, y), s') = T_{\text{base}}(s, a_{\text{base}}, s')$ . An example of a base action could be a desired

movement of the tactile sensor, while the prediction could be the logits of the agent’s current class prediction.

Finally, the reward function is defined as  $R(s, a) = R((s_{\text{base}}, y^*), (a_{\text{base}}, y)) = R_{\text{base}}(s_{\text{base}}, a_{\text{base}}) - \ell(y^*, y)$ , where  $R_{\text{base}}$  is the base reward function and  $\ell$  is a differentiable loss function. An example for a base reward could be an action regularization term, while the loss function  $\ell$  could be a cross-entropy loss in a classification task. Hence, the agent has to make a prediction in every step, encouraging it to gather information quickly to maximize its prediction reward early on. A visualization of this process on the TactileMNIST digit classification task is shown in Fig. 2.

### 3.2 Active Perception Gym

`ap_gym` models active perception tasks as episodic processes in a way that is fully compatible with Gymnasium [21]. Each task is defined as a Gymnasium environment, bundled with the differentiable loss function  $\ell(y^*, y)$  and the prediction target  $y^*$ . Since the loss functions need to convey gradient information to the learning algorithm, we currently provide them either JAX [56] or PyTorch [57] functions, but more autograd frameworks might be supported in the future. During roll-outs, `ap_gym` automatically computes task-dependent metrics, such as accuracy for classification, or Euclidean distance for regression.

`ap_gym` provides a family of lightweight environments designed to isolate core exploration and decision-making behaviors in active perception. As summarized in Table 2, `ap_gym` includes 11 environments spanning both classification and regression tasks. Four progressively harder image-based classification benchmarks (CircleSquare, MNIST, CIFAR-10, TinyImageNet) evaluate an agent’s ability to select informative glimpses from natural or synthetic visuals. Two image-localization tasks (TinyImageNetLoc, CIFAR10Loc) require the agent to infer the position of a limited-field-of-view patch within a larger image. Finally, five non-visual regression tasks — LightDark and four LIDAR-based 2D localization environments (Rooms and Maze) — challenge agents to reduce state uncertainty by navigating procedurally generated maps or lighting fields. Crucially, in the self-localization environments, the agent influences the property it is trying to infer — its position — through its actions. Hence, the prediction target changes over time in these environments, which is an explicitly supported aspect of `ap_gym` environments.

For the image-based classification and localization tasks, `ap_gym` relies on a mix of third-party assets: Tiny ImageNet [3], CIFAR-10 [2], and MNIST [1] datasets. The LIDARLoc (rooms and maze) environments generate map layouts procedurally and require no external data. Whenever applicable, `ap_gym` defines two versions of each environment, one for training with the training split of the respective dataset, and one for evaluation with the test split.

By abstracting away complex contact models and dynamics, `ap_gym` environments enable rapid prototyping of active perception strategies and provide a controlled baseline for more complex scenarios in the TMBS suite. However, despite their simplistic appearance, all `ap_gym` environments impose significant challenges due to partial observability and non-immediate action payoffs. The tasks differ substantially from each other, testing the algorithm’s capability to handle diverse scenarios.

### 3.3 The Tactile MNIST Benchmark Suite

Tactile sensing presents unique challenges for perception: as an interactive modality, touch can unintentionally shift objects during exploration, and modern vision-based tactile sensors, such as GelSight [22] and DIGIT [46], produce inherently high-dimensional observations. At the same time, tactile sensing provides highly localized information confined to points of contact, necessitating active perception.

The Tactile MNIST Benchmark Suite (TMBS) extends `ap_gym` to tactile tasks using vision-based tactile sensors. It contains four environments: *TactileMNIST*, where the agent must classify a 3D model of a hand-written digit (see Section 3.4), *TactileMNISTVolume*, which tasks the agent to infer the volume of a given digit, *Toolbox*, where the agent must estimate the pose of a tool, and

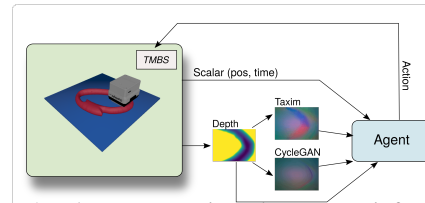


Figure 3: The agent receives the sensory information from the environment. This observation consists of scalar values and a tactile image. This can have three rendering modes, depth, Taxim, or CycleGAN.

*Starstruck*, in which the agent must count the number of stars among other shapes (see Table 2 for an overview). In each environment, the agent controls a simulated GelSight Mini tactile sensor [22] and is presented with one or more objects on a platform. By interacting with the object, the agent must infer task-dependent properties, such as the class of the object, its pose, or its volume. Particularly, aside from tactile data and proprioception, the agent does not receive any additional sensory data, so it has to infer the required property from touch alone. Although, for simplicity and performance reasons, we do not simulate the physical interaction between the sensor and the object, we shift the objects around randomly to simulate unintended object movements.

To simulate the tactile sensor, we support three rendering modes:

- Taxim:** Taxim [55] computes an approximation of the gel deformation and afterwards applies a data-driven rendering algorithm.
- CycleGAN:** With data collected on 3D printed MNIST 3D objects (see Section 3.5), we train a CycleGAN [23] for a style transfer between a depth image and tactile image [58]. The resulting images are visually much more realistic than the Taxim renderings, and thus might be beneficial for sim-to-real transfer. However, this mode is currently only available for the *TactileMNIST* environment. For more details, refer to Appendix C.
- Depth:** Here, the agent receives a depth image clipped to the GelSight gel thickness (4.25mm).

A comparison of all rendering modes is shown in Fig. 3, a visualization of the TactileMNIST digit classification task is provided in Fig. 2, and an overview of all tasks in TMBS is given in Table 2.

### 3.4 The MNIST 3D Dataset

*MNIST 3D*<sup>3</sup> is a collection of 13,580 auto-generated 3D-printable meshes derived from a  $500 \times 500$  pixel high-resolution MNIST variant [59] and scaled to fit in a 10x10cm square. The MNIST 3D dataset poses an exciting tactile classification challenge, as it has significant variability in shape and size within the classes, while also being large enough to facilitate learning from data. A single touch is rarely enough to classify objects from this dataset, as segments of hand-written digits are usually ambiguous. Hence, even after finding the object, the agent has to apply some strategy (e.g., contour following) to gather enough information for a successful classification. In addition to tactile sensing, this dataset could also be used as a benchmark for 3D mesh classification methods. More details on the generation of the MNIST 3D dataset can be found in Appendix D.

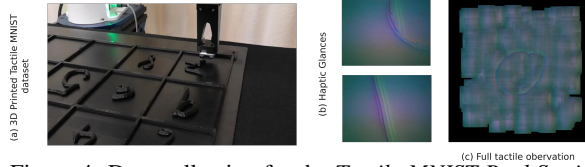


Figure 4: Data collection for the *Tactile MNIST Real Static* dataset. We mounted a GelSight Mini sensor on a Franka Research 3 (a) and collected 153,600 touches across 600 3D-printed MNIST digits. Examples of individual touches are visible in (b), and a collection of 256 touches overlaid based on their positions in (c).

### 3.5 A Large Dataset of Real Tactile Interactions

To complement simulated renders, TMBS includes a real-world, static tactile dataset captured with a GelSight Mini sensor on 3D-printed MNIST 3D digits: the *Real Tactile MNIST Dataset*<sup>4</sup>. The dataset contains video sequences of 153,600 touches across 600 digits, which amounts to 256 touches per object collected in sequence. For data acquisition, we laid each 3D-printed MNIST digit in a 12x12cm grid on a rubber mat and used a Franka Research 3 robot arm [60], with a GelSight Mini tactile sensor to press the sensor down at random locations in the cell. Once we measured a normal force exceeding 5N, we stopped pressing and registered the time stamp. To prevent degradation of the elastomer gel, we replaced the GelSight sensor’s gel pad after every 76,800 touches (i.e., halfway through each dataset). Finally, we partitioned each dataset into training (90 %) and test (10 %) splits, ensuring uniform class distributions across each split. Note that we also provide two processed versions of this dataset, where we replaced the videos with still images at the time of contact, one in full resolution at  $320 \times 240 \text{px}$ <sup>5</sup> and one scaled to  $64 \times 64 \text{px}$ <sup>6</sup> for faster loading and training.

<sup>3</sup> <https://huggingface.co/datasets/TimSchneider42/tactile-mnist-mnist3d>

<sup>4</sup> <https://huggingface.co/datasets/TimSchneider42/tactile-mnist-touch-real-seq-t256-320x240>

<sup>5</sup> <https://huggingface.co/datasets/TimSchneider42/tactile-mnist-touch-real-single-t256-320x240>

<sup>6</sup> <https://huggingface.co/datasets/TimSchneider42/tactile-mnist-touch-real-single-t256-64x64>

We note that an additional challenge introduced during data collection is the possibility of the digit shifting slightly due to contact with the sensor. This variability makes the dataset more representative of real-world scenarios and provides an opportunity for methods to learn robustness to object movement and misalignment. Thus, the Real Tactile MNIST Dataset serves several key roles in the TMBS benchmark. First, it enables training of a CycleGAN for realistic simulation of tactile images and sim-to-real transfer. Second, it can be used for both pretraining and fine-tuning of learning-based perception models, enabling models to acquire basic tactile features before being deployed on a robot for active learning tasks and again facilitating sim-to-real transfer. Finally, the dataset provides a reproducible, offline benchmark for validating and comparing active perception algorithms under realistic sensor noise and material artifacts. For additional details on the data collection procedure, refer to Appendix E.

### 3.6 Evaluation Protocols

In `ap_gym` environments, there are two levels of exploration: (1) during an episode, the agent must explore to gather information, and (2), over the course of the training, the agent must explore the effects of its actions to optimize its model and policy. To disambiguate the measures of performance in these two levels, we will call the first one *exploration efficiency* and the second *sample efficiency*. Importantly, the former is a quality measure of the policy, while the latter is a quality measure of the learning algorithm. Here we borrow the term *sample efficiency* from the RL literature, where it refers to the number of environment interactions the agent needs in order to learn to solve the given task. By *exploration efficiency*, on the other hand, we refer to the efficiency with which the agent collects information within an episode.

Regarding *exploration efficiency*, we consider two measures: the *average* prediction accuracy and the *final* prediction accuracy. Here, *average* prediction accuracy means the prediction accuracy the agent exhibited throughout an episode on average, while *final* prediction accuracy means the accuracy the agent exhibited at the final step of the episode. Normally, the agent starts each episode with little to no information and then keeps gathering information as the episode progresses. Hence, for a rational agent, we expect the prediction accuracy to increase over the course of the episode and to be highest at the end of the episode. Thus, the *average* prediction accuracy could be seen as a measure of how quickly the agent explored, while the *final* prediction accuracy could be seen as a measure of how thoroughly the agent explored throughout the episode. In `ap_gym` environments, both of these measures are tracked for a number of environment-specific prediction accuracy metrics, such as classification accuracy, mean-squared-error, pose error, and others. For a detailed list of metrics for each environment, refer to Appendix F.

Approaches evaluating on `ap_gym` or the Tactile MNIST benchmark suite should report both *average* and *final* metric values over the course of the training. If applicable, the metrics should be computed on the test variants of the environments, which use the test split instead of the training split. The objective is to maximize both *sample efficiency* and *exploration efficiency*. Section 4 serves as an example for an evaluation report on `ap_gym` and Tactile MNIST environments.

## 4 Experiments

In this section, we highlight experiments across selected environments from `ap_gym` and TMBS for various baseline methods, including TAP [52] and HAM [8]. Both TAP and HAM are RL-based active perception methods and, thus, well suited for evaluation on TMBS. The main difference between them is that TAP employs an actor-critic RL approach in combination with a transformer architecture, while HAM relies on a REINFORCE gradient in combination with an LSTM model. TAP provides two variants: TAP-SAC and TAP-CrossQ, based on SAC [61] and CrossQ [62]. We additionally evaluate a baseline that uses TAP’s transformer model with PPO [63], which we call TAP-PP0.

We highlight experiments on four environments in total. In the CircleSquare environment, the agent can move a glimpse around an image and has to find and classify an object that can be either a circle or a square. The TactileMNIST environment tasks the agent to classify MNIST 3D models by touch alone, and in the Starstruck environment, the agent must count the number of stars (1-3) among other objects on the platform. In the Toolbox environment, the agent must find a tool and determine its 2D pose and orientation on the platform. These environments represent a diverse set of challenges, and solving them requires the agent to adopt efficient exploration strategies, which is made evident by the

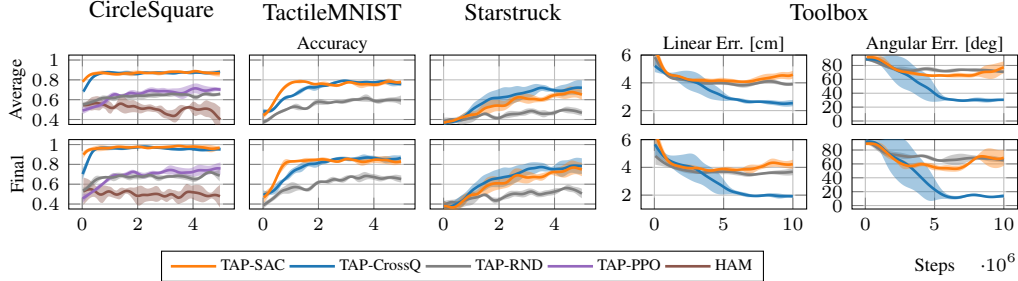


Figure 5: Average and final prediction accuracies for the baseline methods TAP-SAC, TAP-CrossQ, TAP-PP0, HAM [8], and a random baseline TAP-RND for the CircleSquare (ap\_gym), TactileMNIST (TMBS), Starstruck (TMBS), and Toolbox (TMBS) environments. All methods were trained on 5 seeds for up to 10M environment steps. Shaded areas represent one standard deviation. Metrics are computed on evaluation tasks with unseen objects, except for Circle-Square and Toolbox, which have only two and one, respectively. For Starstruck, a correct classification requires predicting the exact number of stars. For Toolbox, we compute the linear and angular displacement between the prediction and the actual object pose as a metric. As HAM does not have a vision encoder, we evaluate it on non-tactile environments only. For TAP-PP0, we found it to be unstable in combination with a vision encoder, so we resort to only evaluating it on non-tactile environments as well.

consistently poor performance of TAP’s random baseline TAP-RND in Fig. 5. Further experiments and details for the training can be found in Appendix G.

As visible in Fig. 5 and Appendix G, TAP’s off-policy methods perform consistently better than the on-policy baselines HAM and TAP-PP0. This gap is likely due to on-policy methods generally being more sample-efficient than off-policy methods, as on-policy methods cannot reuse previously collected samples. However, despite the better performance of TAP, neither the ap\_gym tasks nor the TMBS can be considered solved. TAP requires millions of environment interactions to learn viable exploration policies and falls short of perfect accuracy. More research in the area of sample-efficient RL and active perception is needed to improve sample efficiency to allow for the deployment of such methods in the real world.

## 5 Limitations and Conclusion

In this paper, we have introduced *Active Perception Gym* (ap\_gym), a Gymnasium-compatible benchmark suite tailored for evaluating active perception tasks, and the *Tactile MNIST Benchmark Suite* (TMBS), which contains four tactile-specific tasks designed for robust exploration. To support these benchmarks, we have released a dataset comprising 13,580 high-resolution 3D digit models and an extensive real-world dataset of 153,600 tactile samples collected from 600 3D-printed digits using a GelSight Mini sensor. Provided as an open-source framework, ap\_gym and TMBS offer a structured, standardized, and reproducible benchmark intended to facilitate advancements in active perception research, including efficient exploration strategies, sim-to-real adaptation through CycleGAN training, and the pretraining and fine-tuning of tactile models.

However, our benchmark has limitations, most notably the absence of online, real-world evaluation scenarios and metrics beyond the static dataset. While there are established datasets such as YCB [64] enable benchmarking of contact-rich manipulation tasks using real-world objects, our suite deliberately focuses on controlled, simulation-based exploration to ensure reproducibility and interoperability. In future work, we aim to address this limitation by designing carefully structured real-world tactile exploration experiments that extend the benchmark’s relevance to physical robotic systems and support the study of sim-to-real transfer in active perception. Another key limitation is the absence of a physics engine in our simulation environment, which currently prevents modeling of more complex, contact-rich interactions. As a result, tasks such as grasping, 3D object reconstruction (where objects may tumble upon contact), object retrieval in cluttered scenes, and in-hand pose estimation remain out of scope. Extending our framework to incorporate physics engines would open the door to these richer interaction scenarios and significantly broaden the benchmark’s applicability. Ultimately, we view this benchmark as a foundational resource for advancing active tactile perception and enabling the development of more robust, efficient algorithms for robotic tactile manipulation.

## Acknowledgements

This work was supported by the German Federal Ministry of Education and Research (BMBF) and the French Research Agency, l’Agence Nationale de Recherche (ANR), through the project *Aristotle* (ANR-21-FAI1-0009-01) and the EU’s Horizon Europe project *ARISE* (Grant no.: 101135959). This work is also partly supported by the project *Genius Robot* (01IS24083) funded by the Federal Ministry of Education and Research (BMBF), by the German Research Foundation (DFG, Deutsche Forschungsgemeinschaft) as part of Germany’s Excellence Strategy – EXC 2050/1 – Project ID 390696704 – Cluster of Excellence *Centre for Tactile Internet with Human-in-the-Loop* (CeTI) of Technische Universität Dresden by Bundesministerium für Bildung und Forschung (BMBF), and by the German Academic Exchange Service (DAAD) in project 57616814 (SECAI School of Embedded and Composite AI). The computations were conducted on the IAS Compute Cluster.

## References

- [1] Yann LeCun. The mnist database of handwritten digits. <http://yann.lecun.com/exdb/mnist/>, 1998.
- [2] Alex Krizhevsky, Geoffrey Hinton, et al. Learning multiple layers of features from tiny images. 2009.
- [3] Yann Le and Xuan Yang. Tiny imagenet visual recognition challenge. *CS 231N*, 7(7):3, 2015.
- [4] Roland S Johansson and J Randall Flanagan. Coding and use of tactile signals from the fingertips in object manipulation tasks. *Nature Reviews Neuroscience*, 10(5):345–359, 2009.
- [5] Susan J Lederman and Roberta L Klatzky. Hand movements: A window into haptic object recognition. *Cognitive psychology*, 19(3):342–368, 1987.
- [6] Tony J. Prescott, Mathew E. Diamond, and Alan M. Wing. Active touch sensing. *Phil. Trans. R. Soc. B*, 366(1581):2989–2995, Nov 2011.
- [7] A. Boehm, T. Schneider, B. Belousov, A. Kshirsagar, L. Lin, K. Doerschner, K. Drawing, C.A. Rothkopf, and J. Peters. What matters for active texture recognition with vision-based tactile sensors. In *Proceedings of the IEEE International Conference on Robotics and Automation (ICRA)*, 2024.
- [8] Sascha Fleer, Alexandra Moringen, Roberta L Klatzky, and Helge Ritter. Learning efficient haptic shape exploration with a rigid tactile sensor array. *PloS one*, 15(1):e0226880, 2020.
- [9] Jingxi Xu, Shuran Song, and Matei Ciocarlie. Tandem: Learning joint exploration and decision making with tactile sensors. *IEEE Robotics and Automation Letters*, 7(4):10391–10398, 2022.
- [10] Zhengkun Yi, Roberto Calandra, Filipe Veiga, Herke van Hoof, Tucker Hermans, Yilei Zhang, and Jan Peters. Active tactile object exploration with gaussian processes. In *2016 IEEE/RSJ International Conference on Intelligent Robots and Systems (IROS)*, pages 4925–4930. IEEE, 2016.
- [11] Marten Björkman, Yasemin Bekiroglu, Virgile Högman, and Danica Kragic. Enhancing visual perception of shape through tactile glances. In *2013 IEEE/RSJ International Conference on Intelligent Robots and Systems*, pages 3180–3186. IEEE, 2013.
- [12] Niklas Funk, Erik Helmut, Georgia Chalvatzaki, Roberto Calandra, and Jan Peters. Evetac: An Event-Based Optical Tactile Sensor for Robotic Manipulation. *IEEE Trans. Rob.*, 40:3812–3832, July 2024.
- [13] Justin Kerr, Huang Huang, Albert Wilcox, Ryan Hoque, Jeffrey Ichnowski, Roberto Calandra, and Ken Goldberg. Self-supervised visuo-tactile pretraining to locate and follow garment features. *arXiv preprint arXiv:2209.13042*, 2022.
- [14] Carolina Higuera, Akash Sharma, Chaithanya Krishna Bodduluri, Taosha Fan, Patrick Lancaster, Mrinal Kalakrishnan, Michael Kaess, Byron Boots, Mike Lambeta, Tingfan Wu, and Mustafa Mukadam. Sparsh: Self-supervised touch representations for vision-based tactile sensing. In *8th Annual Conference on Robot Learning*, 2024.

- [15] J. Deng, W. Dong, R. Socher, L.-J. Li, K. Li, and L. Fei-Fei. ImageNet: A Large-Scale Hierarchical Image Database. In *CVPR09*, 2009.
- [16] Tsung-Yi Lin, Michael Maire, Serge Belongie, James Hays, Pietro Perona, Deva Ramanan, Piotr Dollár, and C Lawrence Zitnick. Microsoft coco: Common objects in context. In *Computer Vision–ECCV 2014: 13th European Conference, Zurich, Switzerland, September 6-12, 2014, Proceedings, Part V 13*, pages 740–755. Springer, 2014.
- [17] Andreas Geiger, Philip Lenz, and Raquel Urtasun. Are we ready for autonomous driving? the kitti vision benchmark suite. In *Conference on Computer Vision and Pattern Recognition (CVPR)*, 2012.
- [18] Garrick Brazil, Abhinav Kumar, Julian Straub, Nikhila Ravi, Justin Johnson, and Georgia Gkioxari. Omni3d: A large benchmark and model for 3d object detection in the wild. In *Proceedings of the IEEE/CVF conference on computer vision and pattern recognition*, pages 13154–13164, 2023.
- [19] Sudharshan Suresh, Haozhi Qi, Tingfan Wu, Taosha Fan, Luis Pineda, Mike Lambeta, Jitendra Malik, Mrinal Kalakrishnan, Roberto Calandra, Michael Kaess, et al. Neuralfeels with neural fields: Visuotactile perception for in-hand manipulation. *Science Robotics*, 9(96):ead10628, 2024.
- [20] Amir-Hossein Shahidzadeh, Seong Jong Yoo, Pavan Mantripragada, Chahat Deep Singh, Cornelia Fermüller, and Yiannis Aloimonos. Actexplore: Active tactile exploration on unknown objects. In *2024 IEEE International Conference on Robotics and Automation (ICRA)*, pages 3411–3418. IEEE, 2024.
- [21] Mark Towers, Ariel Kwiatkowski, Jordan Terry, John U Balis, Gianluca De Cola, Tristan Deleu, Manuel Goulão, Andreas Kallinteris, Markus Krimmel, Arjun KG, et al. Gymnasium: A standard interface for reinforcement learning environments. *arXiv preprint arXiv:2407.17032*, 2024.
- [22] Wenzhen Yuan, Siyuan Dong, and Edward H Adelson. Gelsight: High-resolution robot tactile sensors for estimating geometry and force. *Sensors*, 17(12):2762, 2017.
- [23] Jun-Yan Zhu, Taesung Park, Phillip Isola, and Alexei A. Efros. Unpaired image-to-image translation using cycle-consistent adversarial networks, 2020.
- [24] Sabhari Natarajan, Galen Brown, and Berk Calli. Aiding grasp synthesis for novel objects using heuristic-based and data-driven active vision methods. *Frontiers in Robotics and AI*, 8:696587, 2021.
- [25] Qianfan Zhao, Lu Zhang, Lingxi Wu, Hong Qiao, and Zhiyong Liu. A real 3d embodied dataset for robotic active visual learning. *IEEE Robotics and Automation Letters*, 7(3):6646–6652, 2022.
- [26] David Hall, Ben Talbot, Suman Raj Bista, Haoyang Zhang, Rohan Smith, Feras Dayoub, and Niko Sünderhauf. The robotic vision scene understanding challenge. *arXiv preprint arXiv:2009.05246*, 2020.
- [27] Pourya Hoseini, Shuvo Kumar Paul, Mircea Nicolescu, and Monica Nicolescu. Next best view planning in a single glance: An approach to improve object recognition. *SN Computer Science*, 4(1):51, 2022.
- [28] Phil Ammirato, Patrick Poirson, Eunbyung Park, Jana Kosecka, and Alexander C. Berg. A dataset for developing and benchmarking active vision. In *IEEE International Conference on Robotics and Automation (ICRA)*, 2017.
- [29] Phil Ammirato, Alexander C Berg, and Jana Kosecka. Active vision dataset benchmark. In *Proceedings of the IEEE Conference on Computer Vision and Pattern Recognition Workshops*, pages 2046–2049, 2018.



- [30] Jie Wu, Tianshui Chen, Lishan Huang, Hefeng Wu, Guanbin Li, Ling Tian, and Liang Lin. Active object search. In *Proceedings of the 28th ACM International Conference on Multimedia*, pages 973–981, 2020.
- [31] Ziyue Wang, Chi Chen, Fuwen Luo, Yurui Dong, Yuanchi Zhang, Yuzhuang Xu, Xiaolong Wang, Peng Li, and Yang Liu. Actiview: Evaluating active perception ability for multimodal large language models, 2024.
- [32] Tianyi Liu and Benjamin Ward-Cherrier. The tip benchmark: A tactile image-based psychophysics-inspired benchmark for artificial tactile sensors. In *International Conference on Human Haptic Sensing and Touch Enabled Computer Applications*, pages 94–106. Springer, 2024.
- [33] Jialiang Zhao, Yuxiang Ma, Lirui Wang, and Edward H. Adelson. Transferable tactile transformers for representation learning across diverse sensors and tasks, 2024.
- [34] Sudharshan Suresh, Zilin Si, Stuart Anderson, Michael Kaess, and Mustafa Mukadam. Midas-Touch: Monte-Carlo inference over distributions across sliding touch. In *Proc. Conf. on Robot Learning, CoRL*, Auckland, NZ, December 2022.
- [35] Wenzhen Yuan, Yuchen Mo, Shaoxiong Wang, and Edward H Adelson. Active clothing material perception using tactile sensing and deep learning. In *2018 IEEE International Conference on Robotics and Automation (ICRA)*, pages 4842–4849. IEEE, 2018.
- [36] Fengyu Yang, Chenyang Ma, Jiacheng Zhang, Jing Zhu, Wenzhen Yuan, and Andrew Owens. Touch and go: Learning from human-collected vision and touch. *arXiv preprint arXiv:2211.12498*, 2022.
- [37] Shan Luo, Wenzhen Yuan, Edward Adelson, Anthony G Cohn, and Raul Fuentes. Vitac: Feature sharing between vision and tactile sensing for cloth texture recognition. In *2018 IEEE International Conference on Robotics and Automation (ICRA)*, pages 2722–2727. IEEE, 2018.
- [38] Wenzhen Yuan, Shaoxiong Wang, Siyuan Dong, and Edward Adelson. Connecting look and feel: Associating the visual and tactile properties of physical materials. In *Proceedings of the IEEE conference on computer vision and pattern recognition*, pages 5580–5588, 2017.
- [39] Yunzhu Li, Jun-Yan Zhu, Russ Tedrake, and Antonio Torralba. Connecting touch and vision via cross-modal prediction. In *Proceedings of the IEEE/CVF Conference on Computer Vision and Pattern Recognition*, pages 10609–10618, 2019.
- [40] Samson Yu, Kelvin Lin, Anxing Xiao, Jiafei Duan, and Harold Soh. Octopi: Object property reasoning with large tactile-language models. *arXiv preprint arXiv:2405.02794*, 2024.
- [41] Letian Fu, Gaurav Datta, Huang Huang, William Chung-Ho Panitch, Jaimyn Drake, Joseph Ortiz, Mustafa Mukadam, Mike Lambeta, Roberto Calandra, and Ken Goldberg. A touch, vision, and language dataset for multimodal alignment. *arXiv preprint arXiv:2402.13232*, 2024.
- [42] Ning Cheng, Changhao Guan, Jing Gao, Weihao Wang, You Li, Fandong Meng, Jie Zhou, Bin Fang, Jinan Xu, and Wenjuan Han. Touch100k: A large-scale touch-language-vision dataset for touch-centric multimodal representation. *arXiv preprint arXiv:2406.03813*, 2024.
- [43] Ruohan Gao, Yiming Dou, Hao Li, Tanmay Agarwal, Jeannette Bohg, Yunzhu Li, Li Fei-Fei, and Jiajun Wu. The objectfolder benchmark: Multisensory learning with neural and real objects. In *Proceedings of the IEEE/CVF Conference on Computer Vision and Pattern Recognition*, pages 17276–17286, 2023.
- [44] Ruohan Gao, Zilin Si, Yen-Yu Chang, Samuel Clarke, Jeannette Bohg, Li Fei-Fei, Wenzhen Yuan, and Jiajun Wu. Objectfolder 2.0: A multisensory object dataset for sim2real transfer. In *Proceedings of the IEEE/CVF Conference on Computer Vision and Pattern Recognition (CVPR)*, pages 10598–10608, 2022.
- [45] Ruohan Gao, Yen-Yu Chang, Shivani Mall, Li Fei-Fei, and Jiajun Wu. Objectfolder: A dataset of objects with implicit visual, auditory, and tactile representations. *arXiv preprint arXiv:2109.07991*, 2021.

- [46] Mike Lambeta, Po-Wei Chou, Stephen Tian, Brian Yang, Benjamin Maloon, Victoria Rose Most, Dave Stroud, Raymond Santos, Ahmad Byagowi, Gregg Kammerer, et al. Digit: A novel design for a low-cost compact high-resolution tactile sensor with application to in-hand manipulation. *IEEE Robotics and Automation Letters*, 5(3):3838–3845, 2020.
- [47] Zhao-Heng Yin, Binghao Huang, Yuzhe Qin, Qifeng Chen, and Xiaolong Wang. Rotating without seeing: Towards in-hand dexterity through touch. *arXiv preprint arXiv:2303.10880*, 2023.
- [48] Haozhi Qi, Brent Yi, Sudharshan Suresh, Mike Lambeta, Yi Ma, Roberto Calandra, and Jitendra Malik. General in-hand object rotation with vision and touch. In *Conference on Robot Learning*, pages 2549–2564. PMLR, 2023.
- [49] Kenneth Y Goldberg and Ruzena Bajcsy. Active touch and robot perception. *Cognition and Brain Theory*, 7(2):199–214, 1984.
- [50] Ruzena Bajcsy, Yiannis Aloimonos, and John K Tsotsos. Revisiting active perception. *Autonomous Robots*, 42:177–196, 2018.
- [51] Cristiana De Farias, Naresh Marturi, Rustam Stolkin, and Yasemin Bekiroglu. Simultaneous tactile exploration and grasp refinement for unknown objects. *IEEE Robotics and Automation Letters*, 6(2):3349–3356, 2021.
- [52] Tim Schneider, Cristiana de Farias, Roberto Calandra, Liming Chen, and Jan Peters. Active perception for tactile sensing: A task-agnostic attention-based approach, 2025.
- [53] Ruohan Gao, Zilin Si, Yen-Yu Chang, Samuel Clarke, Jeannette Bohg, Li Fei-Fei, Wenzhen Yuan, and Jiajun Wu. Objectfolder 2.0: A multisensory object dataset for sim2real transfer. In *CVPR*, 2022.
- [54] Shaoxiong Wang, Mike Lambeta, Po-Wei Chou, and Roberto Calandra. Tacto: A fast, flexible, and open-source simulator for high-resolution vision-based tactile sensors. *IEEE Robotics and Automation Letters*, 7(2):3930–3937, 2022.
- [55] Zilin Si and Wenzhen Yuan. Taxim: An example-based simulation model for gelsight tactile sensors. *IEEE Robotics and Automation Letters*, 7(2):2361–2368, 2022.
- [56] James Bradbury, Roy Frostig, Peter Hawkins, Matthew James Johnson, Chris Leary, Dougal Maclaurin, George Nécule, Adam Paszke, Jake VanderPlas, Skye Wanderman-Milne, and Qiao Zhang. JAX: composable transformations of Python+NumPy programs, 2018.
- [57] Adam Paszke, Sam Gross, Francisco Massa, Adam Lerer, James Bradbury, Gregory Chanan, Trevor Killeen, Zeming Lin, Natalia Gimelshein, Luca Antiga, Alban Desmaison, Andreas Kopf, Edward Yang, Zachary DeVito, Martin Raison, Alykhan Tejani, Sasank Chilamkurthy, Benoit Steiner, Lu Fang, Junjie Bai, and Soumith Chintala. Pytorch: An imperative style, high-performance deep learning library. In *Advances in Neural Information Processing Systems* 32, pages 8024–8035. Curran Associates, Inc., 2019.
- [58] Weihang Chen, Yuan Xu, Zhenyang Chen, Peiyu Zeng, Renjun Dang, Rui Chen, and Jing Xu. Bidirectional sim-to-real transfer for gelsight tactile sensors with cyclegan. *IEEE Robotics and Automation Letters*, 7(3):6187–6194, 2022.
- [59] Cédric Beaulac and Jeffrey S. Rosenthal. Introducing a new high-resolution handwritten digits data set with writer characteristics. *SN Computer Science*, 4(1), November 2022.
- [60] Franka Inc. Homepage, January 2025. [Online; accessed 28. Jan. 2025].
- [61] Tuomas Haarnoja, Aurick Zhou, Kristian Hartikainen, George Tucker, Sehoon Ha, Jie Tan, Vikash Kumar, Henry Zhu, Abhishek Gupta, Pieter Abbeel, et al. Soft actor-critic algorithms and applications. *arXiv preprint arXiv:1812.05905*, 2018.
- [62] Aditya Bhatt, Daniel Palenicek, Boris Belousov, Max Argus, Artemij Amiranashvili, Thomas Brox, and Jan Peters. Crossq: Batch normalization in deep reinforcement learning for greater sample efficiency and simplicity. *arXiv preprint arXiv:1902.05605*, 2019.

- [63] John Schulman, Filip Wolski, Prafulla Dhariwal, Alec Radford, and Oleg Klimov. Proximal policy optimization algorithms. *arXiv preprint arXiv:1707.06347*, 2017.
- [64] Berk Calli, Arjun Singh, Aaron Walsman, Siddhartha Srinivasa, Pieter Abbeel, and Aaron M. Dollar. The ycb object and model set: Towards common benchmarks for manipulation research. In *2015 International Conference on Advanced Robotics (ICAR)*, pages 510–517, 2015.
- [65] Alexander I Cowen-Rivers, Wenlong Lyu, Rasul Tutunov, Zhi Wang, Antoine Grosnit, Ryan Rhys Griffiths, Alexandre Max Maraval, Hao Jianye, Jun Wang, Jan Peters, et al. Hebo: Pushing the limits of sample-efficient hyper-parameter optimisation. *Journal of Artificial Intelligence Research*, 74:1269–1349, 2022.
- [66] Jonathan Heek, Anselm Levskaya, Avital Oliver, Marvin Ritter, Bertrand Rondepierre, Andreas Steiner, and Marc van Zee. Flax: A neural network library and ecosystem for JAX, 2024.
- [67] Thomas Wolf, Lysandre Debut, Victor Sanh, Julien Chaumond, Clement Delangue, Anthony Moi, Pierric Cistac, Tim Rault, Rémi Louf, Morgan Funtowicz, Joe Davison, Sam Shleifer, Patrick von Platen, Clara Ma, Yacine Jernite, Julien Plu, Canwen Xu, Teven Le Scao, Sylvain Gugger, Mariama Drame, Quentin Lhoest, and Alexander M. Rush. Transformers: State-of-the-art natural language processing. In *Proceedings of the 2020 Conference on Empirical Methods in Natural Language Processing: System Demonstrations*, pages 38–45, Online, October 2020. Association for Computational Linguistics.

# Appendix

## Table of Contents

---

<b>A</b>	<b>Hyperparameter Optimization</b>	<b>16</b>
<b>B</b>	<b>Illustration of Active Perception in the Toolbox Environment</b>	<b>17</b>
<b>C</b>	<b>CycleGAN-based Tactile Rendering</b>	<b>18</b>
<b>D</b>	<b>3D Mesh Dataset Generation Details</b>	<b>19</b>
D.1	MNIST 3D . . . . .	19
D.2	Starstruck . . . . .	20
<b>E</b>	<b>Real Tactile MNIST Dataset</b>	<b>21</b>
<b>F</b>	<b>Environment Details</b>	<b>22</b>
F.1	Evaluation Metrics . . . . .	22
F.2	ap_gym Environments . . . . .	23
F.3	TMBS Environments . . . . .	30
<b>G</b>	<b>Extra Experiments</b>	<b>34</b>
<b>H</b>	<b>Implementation Details</b>	<b>38</b>

---

Table 3: Hyperparameters determined by the HEBO [65] Bayesian optimizer for TAP-SAC and TAP-CrossQ. The *no vision-encoder* configuration was trained on the CircleSquare environment, while the *vision-encoder* configuration was trained on the TactileMNIST environment. Hyperparameters prepended with *Rel.* are relative to the total number of steps throughout the training.

Hyperparameter	TAP-SAC		TAP-CrossQ	
	no vis.-enc.	vis.-enc.	no vis.-enc.	vis.-enc.
Optimizer type	ADAMW	ADAMW	ADAMW	ADAMW
Learning-rate (actor)	$5 \cdot 10^{-5}$	$5 \cdot 10^{-4}$	$1 \cdot 10^{-5}$	$3 \cdot 10^{-4}$
Learning-rate (critic)	$5 \cdot 10^{-4}$	$5 \cdot 10^{-5}$	$1 \cdot 10^{-4}$	$6 \cdot 10^{-5}$
LR-schedule (both)	none	cosine-decay	none	none
Rel. LR cosine warm-up (both)	N/A	0.15	N/A	N/A
Initial UTD	0.75	0.25	5.0	0.25
Final UTD	4.0	1.5	0.5	3.5
Rel. UTD warm-up	0.9	0.4	0.3	0.45

## A Hyperparameter Optimization

To enable a fair comparison of the baseline approaches, we conduct extensive hyperparameter searches with the HEBO [65] Bayesian optimizer. We found that the optimal hyperparameters for each method may vary from environment to environment, in particular, if one environment requires a vision encoder and the other one does not. To address this issue, we optimize two different sets of hyperparameters, one for environments requiring a vision encoder and one for environments that do not, whenever applicable. For an overview of the input modalities of all environments, refer to Table 17.

From each of the two domains (with and without a vision encoder), we pick one environment to tune the hyperparameters on. In particular, we choose CircleSquare as an environment without a vision encoder and TactileMNIST as an environment with a vision encoder. To evaluate the performance of a set of hyperparameters, we run training for a single seed on the respective environment (250K steps on CircleSquare and 2.5M steps on TactileMNIST, except for HAM and PPO, which we train for 1M steps of CircleSquare) and measure the episode returns averaged over the course of the training. Averaging instead of just taking the final returns makes sure that sample efficiency is taken into consideration when evaluating hyperparameters, as two configurations with the same final returns might have taken a significantly different number of environment interactions to reach that performance.

As Bayesian optimization suffers from the curse of dimensionality, we selected a subset of hyperparameters for the hyperparameter search, which we found to be impactful for performance. Specifically, we tune the learning rate of all approaches, and if applicable, the type of learning rate schedule (none, cosine decay, linear), the parameters of the learning rate schedule (number of warm-up steps), and the optimizer used (ADAM, ADAMW, and SGD). For TAP’s off-policy methods, we additionally tune the update-to-data (UTD) schedule, that is, the initial and final UTD ratio, and the number of warm-up steps.

While we were unable to find parameters for HAM that result in meaningful performance, we gained some insights into the influence of these hyperparameters on TAP-SAC and TAP-CrossQ. While both TAP-SAC and TAP-CrossQ reached similar performances on the tasks they were tuned on, we found TAP-CrossQ to be much more robust to unseen environments, as shown in Section 4 and Appendix G. Since there was no significant difference in performance between TAP-CrossQ’s vision-encoder hyperparameters and non-vision-encoder hyperparameters when applied to the CircleSquare task, we chose to proceed using the vision-encoder hyperparameters for all environments to keep the configuration simple.

The results of the hyperparameter search are shown in Table 3.

## B Illustration of Active Perception in the Toolbox Environment

A formal definition of the active perception process, framed as a special case of a POMDP, is presented in Section 3.1. An example of this process in our benchmark suite is shown in Fig. 6, using the Toolbox environment for illustration. At `step-0` of each episode, the environment is initialized and the robot begins from a uniformly sampled random position. At every subsequent step, the agent receives an observation from the previous interaction—typically a tactile image from the GelSight sensor along with the corresponding sensor pose. The agent processes this input to both predict the desired property (e.g., the pose of a wrench) and select a new interaction point.

The robot is then moved to the selected location, where a new observation is acquired. If the episode has not yet terminated, the process repeats: the agent integrates information from the new data point, updates its internal belief, and chooses the next action. At the end of each step, relevant data (observations, predictions, actions) are stored for evaluation.

Over time, the agent learns an effective exploration strategy. In the case of the wrench, for instance, it may discover that interacting with the object’s extremities helps to disambiguate its orientation. Once the episode concludes, we can analyze the stored data to evaluate estimation accuracy and the efficiency of the exploration strategy. For experimental results and benchmarks, refer to Section 4 and additional evaluations in Appendix G.

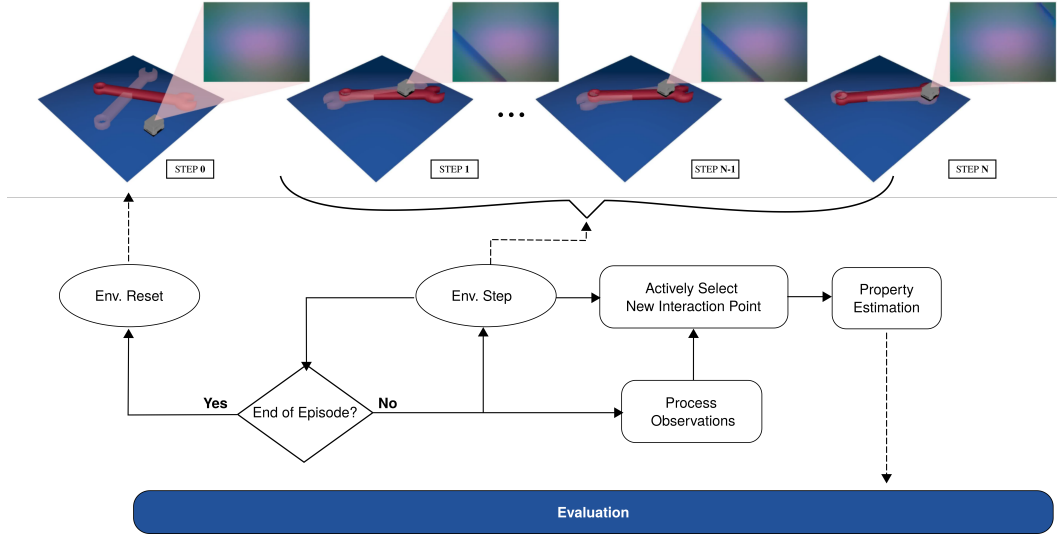


Figure 6: Active perception process in the Toolbox environment.

## C CycleGAN-based Tactile Rendering

The sim2real gap between synthetic and real-world images is a critical challenge for transferring trained algorithms to real-world applications. One approach to generating synthetic tactile images is Taxim [55], an example-based simulator that renders synthetic data from depth maps. However, disparities remain between Taxim’s outputs and real tactile images. While Taxim produces smooth renderings, real tactile images exhibit finer surface textures (e.g., from 3D printing).

To enhance synthetic rendering, we leverage our dataset to train a data-driven image-to-image model. Previous work has demonstrated the effectiveness of such models in bridging the sim2real gap in visual tactile sensors. For instance, [69, 70] employed Pix2Pix [71] to convert synthetic depth maps into realistic images, but this method relies on paired datasets (synthetic-to-real image pairs), which can be expensive to acquire. In contrast, we employ CycleGAN, which has proven effective for tactile renderings [58] and offers two key advantages: first, it supports unpaired training, removing the need for precisely aligned synthetic and real images; second, it enables bidirectional translation, allowing both depth-to-real and real-to-depth synthesis, thereby increasing the model’s flexibility and applicability.

The CycleGAN training dataset was assembled by filtering 20,000 unaligned synthetic depth images and 20,000 real tactile images from our real-world dataset (see Section 3.5 and Appendix E for dataset details) with reduced non-contact data to retain a majority of meaningful images. To address the inherent instability of CycleGAN training, we applied several preprocessing steps. First, we normalized the depth maps: since synthetic depth images encode non-contact images with a default value of 0 (indicating no interaction), we adjusted them to 1 to ensure depth consistency across both contact and non-contact images. Additionally, we converted the 1-channel depth maps into 3-channel heightmaps for better alignment with GelSight RGB images, which are illuminated by side-mounted red, green, and blue LEDs that create a strong correlation between pixel color and spatial position. In this conversion, the first two channels represent the 2D pixel coordinates ( $x$ ,  $y$ ), while the third channel retains the original depth value ( $z$ ). This enhanced representation preserves spatial context during training and enables random cropping - an operation that would otherwise disrupt positional alignment in standard 1-channel depth maps. Qualitative examples of the processed depth maps and CycleGAN results are shown in Fig 7.

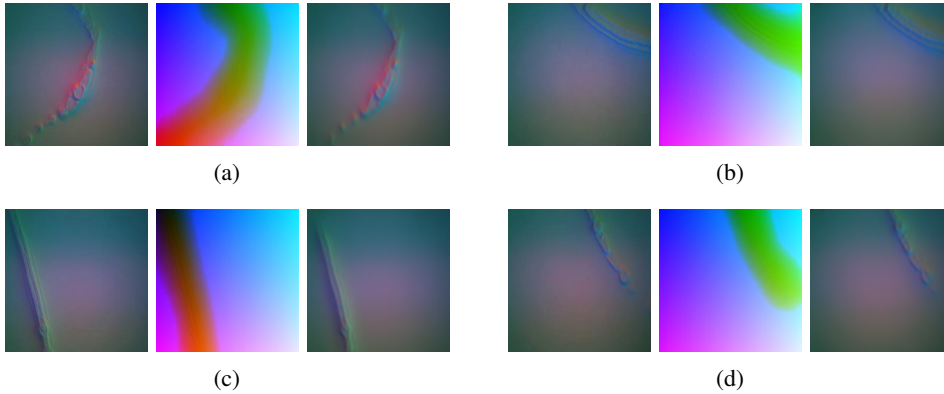


Figure 7: Qualitative results over four cycles illustrating the translation between depth images and RGB images. Each triplet in the figure shows, in order: real tactile (RGB) images, depth images generated using CycleGAN, and the RGB images reconstructed from the generated depth maps. This demonstrates the consistency and reversibility of the RGB-to-depth and depth-to-RGB transformations.



## D 3D Mesh Dataset Generation Details

In this work, we introduce two 3D mesh datasets: MNIST 3D, which contains 3D models of handwritten MNIST digits, and the Starstruck dataset, which contains an arrangement of geometric shapes used in the Starstruck environment. We detail their generation process in the following.

### D.1 MNIST 3D

---

**Algorithm 1** Generating 3D Meshes from High-Resolution MNIST Digits

---

**Require:** High-resolution MNIST digit image  $I$

- 1: Initialize an empty list  $S$
- 2: **for all** erosion size  $k$  in increasing order **do**
- 3:     Apply binary erosion with kernel size  $k$  to  $I$ , yielding  $I_k$
- 4:     Append  $I_k$  to list  $S$
- 5: **end for**
- 6: Stack all  $I_k$  in  $S$  along the depth axis to form 3D tensor  $T$
- 7: Mirror  $T$  along the depth axis to obtain symmetric occupancy grid  $T'$
- 8: Apply Marching Cubes to  $T'$  to extract a surface mesh  $M$
- 9: Smooth mesh  $M$
- 10: Scale  $M$  such that 5 pixels correspond to 1 mm
- 11: **return** Mesh  $M$

---

As described in Appendix D, the MNIST 3D dataset consists of 13,580 auto-generated, 3D-printable meshes derived from the high-resolution MNIST dataset [59]. The mesh generation process is detailed in Algorithm 1. In short, each digit image undergoes iterative binary erosion with increasing kernel sizes to create a series of thinner versions. These eroded images are then stacked into a 3D tensor and mirrored along the third axis to yield a symmetric 3D occupancy grid. Finally, we employ the marching cubes algorithm to convert this grid into a mesh, followed by surface smoothing to enhance mesh quality.

Meshes are scaled such that five pixels correspond to 1 mm, fitting each digit within a bounding box of approximately  $10 \times 10$  cm. In practice, most digit models occupy a smaller volume, as only a few MNIST characters span the full image area. An illustrative subset of the MNIST 3D dataset is shown in Fig. 8.

We split MNIST 3D into five splits, detailed in Table 4.

Table 4: Overview of the splits of the MNIST 3D dataset.

Split	Objects per class	Objects total	Share	Description
train	1,148	11,480	84.5%	Training split. Used by the TactileMNIST environment.
test	100	1,000	7.4%	Test split. Used by the TactileMNIST-test environment.
holdout	50	500	3.7%	Holdout split.
printed_train	50	500	3.7%	Corresponds to the physical 3D-printed digits used in the <i>training</i> split of the Real Tactile MNIST dataset collection.
printed_train	10	100	0.7%	Corresponds to the physical 3D-printed digits used in the <i>test</i> split of the Real Tactile MNIST dataset collection.
Total	1,358	13,580	100%	



Figure 8: The *MNIST 3D* dataset comprises 13,580 3D models of handwritten digits. Each model is auto-generated from a high-resolution MNIST variant [59].

## D.2 Starstruck

In addition to the MNIST digits, we also introduce a dataset of geometric shapes designed for the Starstruck environment. As shown in Fig. 19, each scene may contain squares, circles, and up to three stars. Here, each datapoint corresponds to one arrangement of these geometric shapes.

To generate datapoints, we first choose the number of distractors (circles and squares) randomly between zero and five. We then determine the type of each distractor by randomly choosing between a circle and a square. Afterwards, the distractors and stars are placed on the platform randomly. Beginning with the stars, we place the objects sequentially. For every object, we first sample a uniformly random location on the plate. Whenever a newly placed object would intersect a previously placed object, we sample a new position for the newly placed object. Should this process fail to find a suitable location after 100 attempts, we discard all prior placements and start from scratch.

In total, the Starstruck dataset consists of 3,300 object arrangements, split evenly across the three classes (one, two, and three stars). The test split of this dataset contains 300 objects (100 per class), leaving 3,000 objects (1,000 per class) for the training split.

Table 5: Datapoint structure for the Real Tactile MNIST Dataset.

Field	Description	Type / Shape	Seq	Single
<b>Identification</b>				
id	Unique identifier	int	✓	✓
label	Digit label (0–9)	int	✓	✓
object_id	Original MNIST image ID	int	✓	✓
info	Metadata (e.g. gel type, notes)	dict	✓	✓
<b>Spatial (Cell Frame)</b>				
pos_in_cell	Intended 2D contact positions	$T \times 2$ np.ndarray	✓	✓
gel_pose_cell_frame_seq	Full 3D pose per video frame	list[T] of list[N <sub>i</sub> ] of Transformation	✓	—
gel_pose_cell_frame	3D pose at peak contact	list[T] of Transformation	—	✓
<b>Temporal</b>				
video_length_frames	Frames per clip	list[T] of int	✓	—
time_stamp_rel_seq	Frame timestamps (relative)	list[T] of list[N <sub>i</sub> ] of timedelta	✓	—
touch_start_time_rel	Start of contact	list[T] of timedelta	✓	—
touch_end_time_rel	End of contact	list[T] of timedelta	✓	—
<b>Sensor Data</b>				
sensor_video	Raw video sequences	list[T] of torchvision.io.VideoReader	✓	—
sensor_image	Extracted tactile snapshot	list[T] of np.ndarray	—	✓

**Notes:**  $T$  is the number of touches in a data point;  $N_i$  is the number of frames in the  $i$ -th video.

## E Real Tactile MNIST Dataset

As described in Section 3.5, to collect high-quality, real-world tactile data on 600 3D-printed MNIST digits, we used a Franka Emika Research 3 robot arm equipped with a GelSight Mini tactile sensor. To that end, we replaced the end-effector of the robot with a custom-made 3D-printed mount for the GelSight Mini sensor, as shown in Fig. 4. Following, we further detail the data collection protocol as well as the datapoint structure for our dataset.

### Data Collection Protocol

Each of the 600 3D-printed MNIST digits was placed in a  $12 \times 12$  cm cell on a rubber mat. The robot moved systematically across the dataset, visiting one digit at a time and performing 256 distinct tactile interactions per object. For each interaction, a target location was sampled randomly within the cell, and the robot was commanded to lower the sensor perpendicularly onto the digit’s surface. The coordinate frame of each cell was defined in the center with the x-axis pointing to the right of the robot, the y-axis pointing away from the robot, and the z-axis pointing up, orthogonal to the cell.

The tactile interaction was terminated automatically when the robot detected a normal force exceeding 5 N. At this point, the timestamp of contact was registered, and the sequence was recorded. This force threshold was chosen to ensure consistent contact without damaging the elastomer or over-deforming the object geometry. Note, however, that the Franka robot does not have force sensors in its wrist and instead relies on torque sensors in its joints and a dynamics model to compute the acting forces. Depending on the pose of the robot, this force estimate varies in accuracy, which is why the force being applied to the object is not guaranteed to be consistent.

To maintain data quality and preserve sensor integrity, the elastomer gel pad of the GelSight sensor was replaced halfway through the data collection process (after 76,800 touches). This helped mitigate the impact of gel degradation on the quality of the tactile readings.

### Dataset Structure

The dataset contains a total of 153,600 tactile interactions ( $600 \text{ digits} \times 256 \text{ touches}$ ). These are stored as video sequences capturing the contact event from the moment the sensor begins moving towards the digit until full contact is achieved and the interaction is complete.

We provide two formats of this dataset:

- **Sequence data-points** (`seq`): Each touch is stored as a short video, capturing the dynamic contact event.
- **Single-image data-points** (`single`): Each touch is represented by a single frame extracted at the moment of contact.

Each data point in both formats represents a group of 256 touches per digit and includes metadata for downstream use in learning-based or analytical tasks. Each "`seq`" data point contains fine-grained temporal and spatial information about the tactile interaction, useful for modeling contact dynamics or time-series prediction. The "`single`" variant simplifies data loading and reduces computational overhead. A summary of the data fields is shown in Table 5.

## F Environment Details

In this section, we provide a more detailed description of each environment included in our framework, along with the metrics used to evaluate them within the context of our benchmark protocol. Notably, both `ap_gym` and `TMBS` encompass tasks that can be categorized as either regression or classification (see Table 2 for an overview). Accordingly, we organize the evaluation metrics into two groups: classification metrics and regression metrics.

### F.1 Evaluation Metrics

`ap_gym` and `TMBS` automatically track a variety of metrics for the different environments. Depending on the type of task (classification or regression), different metrics are tracked. We briefly explain all tracked metrics in Table 6.

For further details, refer to Section 3.6.

Table 6: Overview of all evaluation metrics computed by `ap_gym` and `TMBS`.

Environment type	Metric name	Step-based	Description
Classification	Accuracy	✓	Can either be zero or one in each step. One if the correct label has the highest predicted probability, else zero.
	Correct label prob.	✓	Probability of the correct label in the prediction of the agent.
	First correct class.	✗	Step relative to the start of the episode, at which the agent predicted the correct class for the first time. If there is no correct prediction in an episode, this metric is not computed.
	Last incorrect class.	✗	Step relative to the start of the episode, at which the agent predicted an incorrect class for the last time.
Regression	Mean-squared error	✓	Mean-squared error between the agent’s prediction and the ground truth value.
	Euclidean distance	✓	Square root of the mean-squared error.
Toolbox	Linear error	✓	The distance between the predicted object position and the actual object position.
	Angular error	✓	The angle between the predicted object orientation and the actual object orientation.
TactileMNISTVol.	Relative error	✓	Predicted volume divided by the actual volume of the object.

## F.2 ap\_gym Environments

The ap\_gym environments are mainly divided into image classification tasks, 2D localization tasks and image-patch localization tasks. Following, we detail each of these.

### F.2.1 Image Classification Task

In the image classification environments, an agent must classify an image by navigating through it using a small glimpse window. This glimpse is never large enough to capture the full image in a single view, necessitating sequential exploration to accumulate sufficient information. As can be seen in Fig. 11–12, the current agent’s glimpse is marked in blue. Additionally, the agent’s previous glimpses are visualized with a color gradient from red to green, where red indicates a predicted probability of 0 for the correct class, and green indicates a predicted probability of 1. All image classification environments in ap\_gym share the properties described in Table 7.

Table 7: Environment specifications shared by all image classification tasks.

Property	Specification
<b>Action Space</b>	The action $\mathbf{A} \in [-1, 1]^2$ describes the relative movement of the glimpse sensor. The value is first projected into the unit circle and then scaled by 0.2 (10 % of the image), before being added to the current sensor position.
<b>Prediction Space</b>	Agent outputs logits $\mathbf{Y} \in \mathbb{R}^K$ corresponding to predicted probabilities for each class label.
<b>Prediction Target Space</b>	True label $Y^* \in \{0, \dots, K - 1\}$ .
<b>Observation Space</b>	The observation space is a dictionary with the following keys: <ul style="list-style-type: none"> <li><b>glimpse</b>: a tensor <math>\in [0, 1]^{G \times G \times C}</math> that represents a glimpse of the image.</li> <li><b>glimpse_pos</b>: a vector <math>\in [-1, 1]^2</math> that contains the normalized position of the glimpse within the image.</li> <li><b>time_step</b>: a scalar <math>\in [-1, 1]</math> that represents the normalized current time step between 0 and the step limit.</li> </ul>
<b>Loss Function</b>	Cross entropy loss
<b>Reward Function</b>	At each step, the sum of: <ol style="list-style-type: none"> <li><math>10^{-3} \cdot \ \mathbf{a}_t\ </math> (action regularization).</li> <li>Negative cross-entropy loss between prediction and target.</li> </ol>
<b>Initialization</b>	The glimpse starts at a uniformly random position within the image.
<b>Termination</b>	The episode ends with the terminate flag set if the step limit (16) is reached.

**Notation:**  $K \in \mathbb{N}$  is the number of classes;  $G \in \mathbb{N}$  is the glimpse size;  $C \in \mathbb{N}$  is the number of image channels (1 = grayscale, 3 = RGB).

## Implemented Environments

The implemented image classification environments from ap\_gym are detailed in Table 8.

Table 8: Available image classification environments in ap\_gym.

Environment ID	Type	Samples	Size	Glimpse	Step Limit	Classes	Description
CircleSquare	Grayscale	1,568	28x28	5x5	16	2	Images of either a circle or square
MNIST	Grayscale	60,000	28x28	5x5	16	10	Handwritten MNIST [1] digits
CIFAR10	RGB	50,000	32x32	5x5	16	10	CIFAR10 [2] natural images
TinyImageNet	RGB	100,000	64x64	10x10	16	200	TinyImageNet [3] natural images

**CircleSquare:** In this environment, the agent must distinguish between a circle and a square present anywhere in the environment. As shown in Fig. 9, a color gradient guides the agent towards the object. The main challenge in CircleSquare is its sparse-reward nature, in that the agent must learn to take many steps before gaining any information.

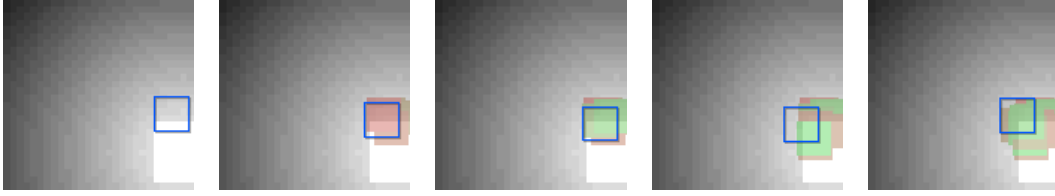


Figure 9: Sequence of glimpses taken by the agent in the CircleSquare environment. Here we show the variation with the gradient.

**MNIST:** In this environment, the agent must classify MNIST [1] digits with partial visibility. In contrast to CircleSquare, the agent generally receives information more quickly, but always sees an incomplete picture and, thus, must learn contour following strategies to gather enough information for a successful classification. This environment contains the train and test variants. In Fig. 10 we show one episode of the MNIST environment.

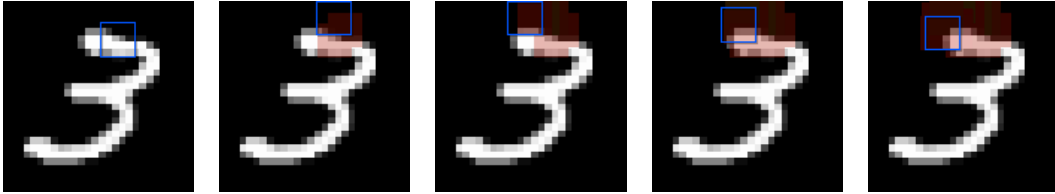


Figure 10: Sequence of glimpses taken by the agent in the MNIST environment on the test set. We show a failed episode here, as can be seen by the red window representing the agent's glance.

**CIFAR10:** This environment (see Fig. 11) challenges the agent to classify CIFAR10 images by sequentially observing glimpses. In contrast to the MNIST environment, the data of CIFAR10 is much more diverse and complex. This environment has the train and test variants.



Figure 11: Sequence of glimpses taken by the agent in the CIFAR10 environment.

**TinyImageNet:** This environment increases classification difficulty due to larger images and a greater number of classes. The higher-resolution data requires more sophisticated exploration strategies. Variants of this environment include the train and test splits. In Fig. 12 we show snapshots of an episode in the TinyImageNet environment.



Figure 12: Sequence of glimpses taken by the agent in the TinyImageNet environment.

## F.2.2 2D Localization environments

In the 2D localization task, an agent must predict its own position by actively exploring its surroundings. Generally, our 2D localization environment can be divided into the following types:

- *LightDark*: the agent must estimate its position based on noisy observations, where the noise level depends on the brightness of the surrounding area.
- *Static LIDAR environments*: The agent is placed at a random position in a fixed 2D bitmap map, with white pixels denoting free space and black pixels indicating obstacles. At each step, it receives 8-beam LIDAR distance readings and exact odometry. Since the map remains constant across episodes, the agent can gradually learn its layout to improve localization.
- *Dynamic LIDAR environments*: Each episode begins with a procedurally generated random map, ensuring minimal repetition. To enable localization in these unseen maps, the full map is provided as part of the observation. As in the static case, the agent also receives 8-beam LIDAR data and odometry at each step.

Examples of agent trajectories in all four LIDAR tasks are shown in Fig. 13–Fig. 14. An episode of the Light–Dark task is shown in Fig. 15. Additionally, all 2D localization tasks share the common properties described in Table 9.

Table 9: Properties of 2D localization environments in `ap_gym`.

Property	LIDAR Environments	Light–Dark Environment
<b>Action Space</b>	Describes the agent’s relative movement. The action, $\mathbf{a} \in [-1, 1]^2$ , is projected onto the unit circle and added to the position (in pixels).	Describes the agent’s relative movement. The action, $\mathbf{a} \in [-1, 1]^2$ , is projected onto the unit circle and scaled by 0.15.
<b>Prediction Space</b>	$\mathbf{Y} \in \mathbb{R}^2$ (normalized predicted position of the agent).	$\mathbf{Y} \in \mathbb{R}^2$ (predicted position of the agent).
<b>Prediction Target</b>	$\mathbf{Y}^* \in \mathbb{R}^2$ (normalized true agent position).	$\mathbf{Y}^* \in \mathbb{R}^2$ (true agent position).
<b>Observation Space</b>	<p>The observation space is a dictionary with the following keys:</p> <ul style="list-style-type: none"> <li>• <code>lidar</code>: a vector <math>\in [0, 1]^8</math> that contains distances measured by the LIDAR sensor</li> <li>• <code>odometry</code>: a vector <math>\in [-1, 1]^2</math> with the agent’s normalized relative displacement.</li> <li>• <code>time_step</code>: a scalar <math>\in [-1, 1]</math> that represents the normalized current time step between 0 and the step limit.</li> <li>• <code>map</code>: a vector <math>\in [0, 1]^{M \times M \times 1}</math> with a grayscale image representation of the environment (dynamic maps only). <math>M \in \mathbb{N}</math> is the map size.</li> </ul>	<p>The observation space is a dictionary with the following keys:</p> <ul style="list-style-type: none"> <li>• <code>noisy_position</code>: a vector <math>\in [-2, 2]^2</math> that contains a noisy estimate of the agent’s position depending on the brightness of the area the agent is in.</li> <li>• <code>time_step</code>: a scalar <math>\in [-1, 1]</math> that represents the normalized current time step between 0 and the step limit.</li> </ul>
<b>Loss Function</b>	Mean Square Error	Mean Square Error
<b>Reward Function</b>	<p>At each step, the sum of:</p> <ol style="list-style-type: none"> <li>1. <math>10^{-3} \cdot \ \mathbf{a}_t\ </math> (action regularization);</li> <li>2. The negative mean squared error between the agent’s prediction and its true position.</li> </ol>	<p>At each step, the sum of:</p> <ol style="list-style-type: none"> <li>1. <math>10^{-3} \cdot \ \mathbf{a}_t\ </math> (action regularization);</li> <li>2. A constant reward of 0.1 to ensure that the reward stays positive and the agent does not learn to terminate the episode on purpose.</li> <li>3. The negative mean squared error between the agent’s prediction and its true position.</li> </ol>
<b>Initialization</b>	The agent begins at a uniformly random, valid location within the environment.	The agent’s initial position is uniformly randomly sampled from the range $[-1, 1]^2$
<b>Termination</b>	The episode ends if either the step limit is reached.	The episode ends if either the step limit is reached or the agent moves out of bounds.

## Implemented Environments

The implemented 2D localization environments from `ap_gym` are detailed in Table 10.



Table 10: Available 2D localization environments in `ap_gym`.

Environment ID	Map Type	Static?	Size	Description
LIDARLocRoomsStatic	Rooms	Yes	32×32	Static rooms.
LIDARLocRooms	Rooms	No	32×32	Random rooms each episode.
LIDARLocMazeStatic	Maze	Yes	21×21	Static maze.
LIDARLocMaze	Maze	No	21×21	Random maze each episode.
LightDark	Light-Dark	No	continuous	Localization with brightness-varying noise.

**LIDARLocRoomsStatic:** In the LIDARLocRoomsStatic environment (see Fig. 13), the agent must localize itself with LIDAR sensors in a map with wide open areas. As the open areas are large, it often does not receive any information from its LIDAR sensors (e.g., when it is in the middle of the room). The agent, therefore, must navigate around the map to gather information and localize itself. In this version of the environment, the map stays constant, meaning that the agent can memorize the layout of the rooms over the course of the training.

**LIDARLocRooms:** In the LIDARLocRooms localization task, shown in Fig. 13, the agent explores larger open areas which have sparse LIDAR readings —especially near the center of rooms. In this version, the room layout changes every episode, meaning that the agent has to learn to process the map it is provided as additional input.

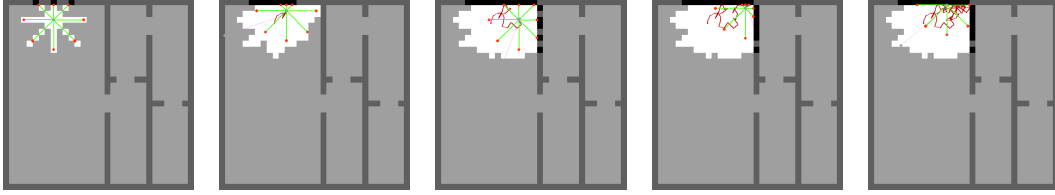


Figure 13: Agent trajectory in the Room Localization environment. Here we see the 8 LIDAR beams extending from the agent, with sparse rewards when the agent is further away from the walls. The purple dot is the agent’s predicted pose, and the line representing the path the agent has taken is encoded with a gradient from red to green, where red indicates a high predicted error and green indicates lower error.

**LIDARLocMazeStatic:** In the LIDARLocMazeStatic environment, the agent has to localize itself with LIDAR sensors in a map with narrow corridors. As the corridors are narrow, it will always receive information from its LIDAR sensors, but many regions of the maze look alike. The agent must therefore navigate around the map to gather information. In this variant, the map stays constant, meaning that the agent can memorize the layout of the maze over the course of the training. In Fig. 14 we show a visualization of this environment.

**LIDARLocMaze:** In this variant of the environment (Fig. 14), the agent navigates procedurally generated mazes with narrow corridors. These layouts change every episode, so the agent receives the full map as part of its observation. Despite always receiving LIDAR readings (due to proximity to walls), the similarity of many areas makes localization challenging.

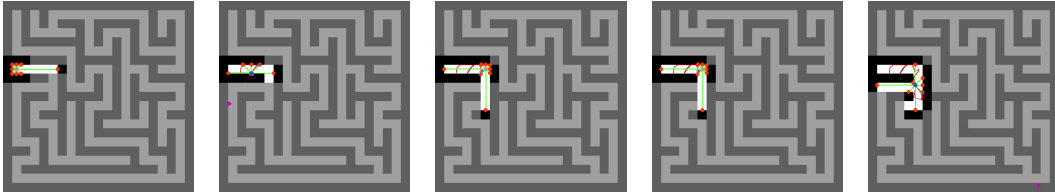


Figure 14: Agent trajectory in the LIDARLocMazeStatic environment, where walls are narrow but similar. The purple dot is the agent’s predicted pose, and the line representing the path the agent has taken is encoded with a gradient from red to green, where red indicates a high predicted error and green indicates lower error.

**LightDark:** In the LightDark-v0 environment (Fig. 15), the agent must estimate its position using noisy observations, where observation noise depends on the brightness of the region it is in. Bright areas yield low-variance signals while dark regions introduce greater uncertainty. The agent

can move toward light to improve accuracy. What makes this environment particularly challenging is that the agent must learn to move towards the light without knowing its own precise position. Hence, it faces uncertainty not only with regard to its prediction, but also the outcomes of its action.

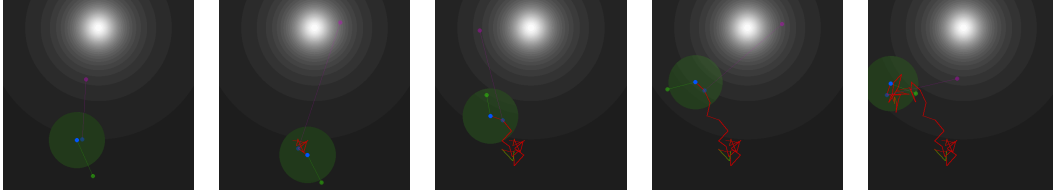


Figure 15: Agent trajectory in the LightDark environment. The blue dot indicates the agent’s current position, while the light blue dot marks its previous position (i.e., the target for prediction). The purple dot shows the agent’s last prediction, and the green dot is the noisy observation the agent receives. The green transparent circle around the agent reflects observation uncertainty, which is higher in dark regions and lower in bright ones. The background encodes environmental visibility: white areas correspond to low-noise (bright) regions, and dark areas to high-noise (dark) regions. The line representing the path the agent has taken is encoded with a gradient from red to green, where red indicates a high predicted error and green indicates lower error.

### F.2.3 Image localization environments

In the image localization environments, an agent must localize a target glimpse within a larger image by moving a small observation window. Since the glimpse cannot cover the full image at once, the agent must navigate sequentially to gather sufficient context and then regress the coordinates of the target region. As shown in Fig. 17, the agent’s current glimpse is outlined in blue, the target glimpse in transparent purple, and the agent’s prediction as an opaque purple box. Past glimpses are colored from red (large error) to green (small error) according to how close each prediction was to the true target. All image localization environments in `ap_gym` share the properties in Table 11.

Table 11: Shared properties of all image localization tasks.

Property	Specification
<b>Action Space</b>	The action $\mathbf{A} \in [-1, 1]^2$ , projected onto the unit circle and scaled by a maximum step length (default 0.20 of image size), describes the relative movement of the glimpse sensor.
<b>Prediction Space</b>	$\mathbf{Y} \in \mathbb{R}^2$ contains the agent’s prediction of the target glimpse position.
<b>Prediction Target</b>	$\mathbf{Y}^* \in \mathbb{R}^2$ contains the true position of the target glimpse.
<b>Observation Space</b>	The observation is a dictionary with the following keys: <ul style="list-style-type: none"> <li><code>glimpse</code>: a vector <math>\in [0, 1]^{G \times G \times C}</math> that represents a glimpse of the image.</li> <li><code>glimpse_pos</code>: a vector <math>\in [-1, 1]^2</math> that contains the normalized position of the glimpse within the image.</li> <li><code>target_glimpse</code>: a vector <math>\in [0, 1]^{G \times G \times C}</math> that represents the target glimpse.</li> <li><code>time_step</code>: a scalar <math>\in [-1, 1]</math> that represents the normalized current time step between 0 and the step limit.</li> </ul>
<b>Loss Function</b>	Mean squared error
<b>Reward Function</b>	At each step, the sum of: <ol style="list-style-type: none"> <li><math>10^{-3} \cdot \ \mathbf{a}_t\ </math> (action regularization).</li> <li>The negative mean squared error between the agent’s prediction and the true coordinates of the target glimpse.</li> </ol>
<b>Initialization</b>	The agent starts at a uniformly random position within the image.
<b>Termination</b>	The episode ends if either the step limit is reached.

**Notation:**  $G \in \mathbb{N}$  is the glimpse size;  $C \in \mathbb{N}$  is the number of image channels (1 = grayscale, 3 = RGB).

### Implemented Environments

The available image localization environments are listed in Table 12.

Table 12: Image localization environments in `ap_gym`.

Environment ID	Type	Samples	Image Size	Glimpse	Steps	Channels	Description
CIFAR10Loc	RGB	50 000	32×32	5×5	16	3	CIFAR10 [2] natural images.
TinyImageNetLoc	RGB	100 000	64×64	10×10	16	3	TinyImageNet [3] natural images.

**CIFAR10Loc:** In CIFAR10Loc (see Fig. 16), the agent must localize a given 5×5 patch within a 32×32 RGB image. Limited visibility forces a strategic search for the target glimpse to reduce localization error.



Figure 16: Agent trajectory in CIFAR10Loc. The blue window represents the current glimpse, in transparent purple we have the target, and the opaque purple box shows the prediction. a gradient from red to green, where red indicates a high predicted error and green indicates a lower error.

**TinyImageNetLoc:** Similar to the CIFAR10Loc, in TinyImageNetLoc (Fig. 17), the agent’s task is to localize a given glimpse in a natural image. However, the greater resolution and diversity make localization more challenging than CIFAR10Loc.

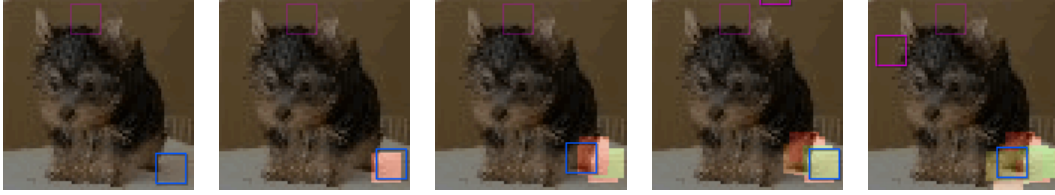


Figure 17: Agent trajectory in TinyImageNetLoc. The blue window represents the current glimpse, in transparent purple we have the target, and the opaque purple box shows the prediction. a gradient from red to green, where red indicates a high predicted error and green indicates a lower error.

### F.3 TMBS Environments

The Tactile MNIST Benchmark Suite (TMBS) is designed to evaluate the efficiency of active tactile perception strategies, testing an agent’s ability to strategically explore, classify, and localize objects while minimizing the number of interactions. As described in Section 3.3, TMBS provides a unified framework based on a simulated GelSight Mini tactile sensor [22], supporting three rendering modes: Taxis, CycleGAN, and Depth. For visualization, the sensor, object, and platform where the object is placed are rendered in 3D. Although the physical interaction between sensor and object is not simulated, object positions are randomly shifted to emulate tactile interaction. Our suite includes four distinct environments covering both classification and regression tasks. Namely: (i) *TactileMNIST* for digit classification, (ii) *TactileMNISTVolume* for digit volume estimation, (iii) *Starstruck* for shape counting, and (iv) *Toolbox* for pose estimation. These are detailed in the next sections.

#### F.3.1 Classification environments

In tactile classification environments, the agent has to classify a 3D object by exploring it with a GelSight Mini tactile sensor. The agent does not have access to the object’s location or orientation, and also receives no visual input. Instead, it must actively control the sensor to find and classify the object. In Table 13 we detail the main environment specifications.

Table 13: Shared properties of all tactile classification environments.

Property	Specification
<b>Action Space</b>	The action space $\mathbf{A}$ is a dictionary with the following keys: <ul style="list-style-type: none"> <li><code>sensor_target_pos_rel</code>: a vector <math>\in [0, 1]^3</math> containing the normalized relative linear target movement.</li> </ul>
<b>Prediction Space</b>	Agent outputs logits $\mathbf{Y} \in \mathbb{R}^K$ corresponding to predicted probabilities for each class label.
<b>Prediction Target Space</b>	True label $Y^* \in \{0, \dots, K - 1\}$ .
<b>Observation Space</b>	The observation space is a dictionary with the following keys: <ul style="list-style-type: none"> <li><code>sensor_img</code>: a tensor <math>\in [-1, 1]^{64 \times 64 \times 3}</math> representing the tactile image from the GelSight sensor.</li> <li><code>sensor_pos</code>: a vector <math>\in [-1, 1]^3</math> indicating the normalized position of the sensor in the workspace.</li> <li><code>time_step</code>: a scalar <math>\in [-1, 1]</math> representing the normalized current time step.</li> </ul>
<b>Loss Function</b>	Cross entropy loss
<b>Reward Function</b>	At each step, the sum of: <ol style="list-style-type: none"> <li><math>10^{-3} \cdot \ a_t\ </math> (action regularization).</li> <li>Negative cross-entropy loss between prediction and target.</li> </ol>
<b>Initialization</b>	The tactile sensor starts at a randomly sampled pose in the workspace.
<b>Termination</b>	The episode ends with the terminate flag set if the step limit is reached.

**Notation:**  $K \in \mathbb{N}$  is the number of classes.

### Implemented Environments

The implemented tactile classification environments from TMBS are detailed in Table 8.

Table 14: Available tactile classification environments in `ap_gym`.

Environment ID	Dataset	Classes	Steps	Perturbation	Description
TactileMNIST	MNIST 3D	10	16	Yes	Classify objects from the <i>MNIST 3D</i> dataset using tactile feedback.
Starstruck	3D shapes	3	32	No	Count the number of stars in a tactile scene.

**TactileMNIST:** In this environment (see Fig. 18 for an episode of the TactileMNIST environment), the agent must classify 3D models of handwritten digits by touch alone. See Section 3.4 for a description of the MNIST 3D dataset. Starting from a random pose, it first locates the digit and then follows its contour to accumulate shape information. With the object perturbation enabled, the digit shifts slightly under the sensor, requiring robust strategies that are invariant to these small shifts in the object’s pose. Variations of this environment include the test and train split, as well as the three rendering modes — CycleGAN, Taxim, and Depth.

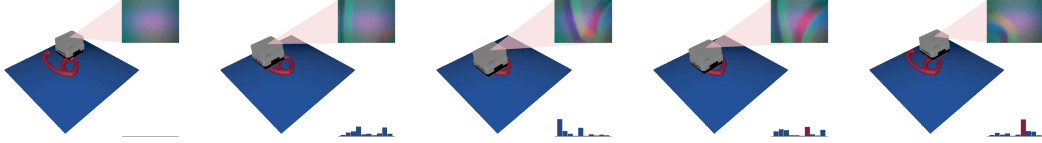


Figure 18: Sequence of tactile glimpses taken by the agent in the TactileMNIST classification environment. The agent observes only local tactile glimpses and its own position. As it actively explores the 3D digit surface, its prediction confidence increases, driven by accumulating shape information. The probabilities for each label are displayed on the bar plot on the side.

**Starstruck:** In the Starstruck environment (see Fig. 19), the agent must count the number of stars in a scene cluttered with other geometric objects, including circles and squares. Since all stars look the same, distinguishing stars from other objects is straightforward. Instead, the main challenge posed in this environment is to learn an effective search strategy to systematically cover as much space as possible. Here, the scenes are prearranged and provided in a small dataset. Variations include the test and train variants, as well as depth and Taxim renderings.

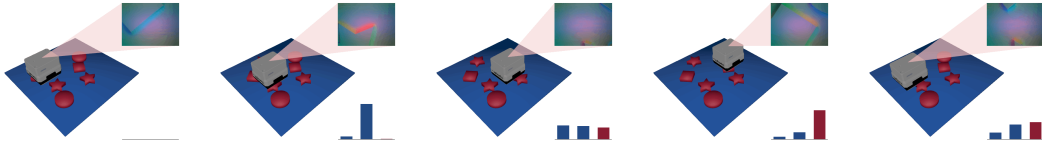


Figure 19: Sequence of tactile glimpses taken by the agent in the Starstruck counting task. The agent perceives only local tactile information and its own position as it explores the scene. To accurately estimate the number of stars, it must develop an efficient search strategy. The presence of distractor shapes (e.g., circles and squares) and scene clutter increases the difficulty of the task. On the side of each episode, the probabilities of each label are shown.

### F.3.2 Regression Environments

In tactile regression environments, the agent must infer a continuous property of a 3D object by exploring it with a GelSight Mini tactile sensor. The agent receives no visual input or ground-truth pose; instead, it must actively control the sensor to locate and explore the object.

All tactile regression environments share the properties in Table 15.

Table 15: Shared properties of all tactile regression environments.

Property	Toolbox	TactileMNISTVolume
<b>Action Space</b>	The action space $\mathbf{A}$ is a dictionary with the following keys: <ul style="list-style-type: none"> <li><code>sensor_target_pos_rel</code>: a vector <math>\in [0, 1]^3</math> containing the normalized relative linear target movement.</li> </ul>	The action space $\mathbf{A}$ is a dictionary with the following keys: <ul style="list-style-type: none"> <li><code>sensor_target_pos_rel</code>: a vector <math>\in [0, 1]^3</math> containing the normalized relative linear target movement.</li> </ul>
<b>Prediction Space</b>	$\mathbf{Y} \in \mathbb{R}^4$ representing the normalized predicted position of the agent, which includes the 2D position in the platform and sine and cosine of the wrench rotation around the up-facing Z-axis.	$\mathbf{Y} \in \mathbb{R}^2$ (predicted position of the agent).
<b>Prediction Target</b>	$\mathbf{Y}^* \in \mathbb{R}^2$ representing the normalized true agent position, with 2D position and sine and cosine around the Z axis.	$\mathbf{Y}^* \in \mathbb{R}^2$ (true agent position).
<b>Observation Space</b>	The observation space is a dictionary with the following keys: <ul style="list-style-type: none"> <li><code>sensor_img</code>: a tensor <math>\in [-1, 1]^{64 \times 64 \times 3}</math> representing the tactile image from the GelSight sensor.</li> <li><code>sensor_pos</code>: a vector <math>\in [-1, 1]^3</math> indicating the normalized position of the sensor in the workspace.</li> <li><code>time_step</code>: a scalar <math>\in [-1, 1]</math> representing the normalized current time step.</li> </ul>	The observation space is a dictionary with the following keys: <ul style="list-style-type: none"> <li><code>sensor_img</code>: a tensor <math>\in [-1, 1]^{64 \times 64 \times 3}</math> representing the tactile image from the GelSight sensor.</li> <li><code>sensor_pos</code>: a vector <math>\in [-1, 1]^3</math> indicating the normalized position of the sensor in the workspace.</li> <li><code>time_step</code>: a scalar <math>\in [-1, 1]</math> representing the normalized current time step.</li> </ul>
<b>Loss Function</b> <b>Reward Function</b>	Mean squared error. At each step, the sum of: <ol style="list-style-type: none"> <li><math>10^{-3} \cdot \ \mathbf{a}_t\ </math> (action regularization).</li> <li>the loss of the current prediction of the agent.</li> </ol>	Mean squared error. At each step, the sum of: <ol style="list-style-type: none"> <li><math>10^{-3} \cdot \ \mathbf{a}_t\ </math> (action regularization).</li> <li>the loss of the current prediction of the agent.</li> </ol>
<b>Initialization</b>	The glimpse starts at a uniformly random position within the workspace.	The glimpse starts at a uniformly random position within the workspace.
<b>Termination</b>	The episode ends with the terminate flag set if the step limit is reached.	The episode ends with the terminate flag set if the step limit is reached.

### Implemented Environments

The implemented tactile regression environments from `ap_gym` are detailed in Table 16.

Table 16: Available tactile regression environments in `ap_gym`.

Environment ID	Dataset	$N$	Steps	Perturbation	Description
Toolbox	3D Tools	4	64	Yes	Estimate the 2D position and orientation of a tool (e.g., wrench) placed in the environment.
TactileMNISTVolume	MNIST 3D	1	32	Yes	Estimate the normalized volume of a MNIST 3D digit model.

**Toolbox:** In the Toolbox environment (see Fig. 20), the agent must locate a tool on a platform and regress its canonical 2D coordinates and orientation. Touching only the handle or head yields partial information, so the agent must explore, strategically seeking out the wrench’s ends to resolve



ambiguities and accurately estimate its pose. Here, the pose is described as a 4D vector, with the 2D  $(x, y)$  coordinates in the platform, and the Z-axis rotation is represented as a 2D sine and cosine.

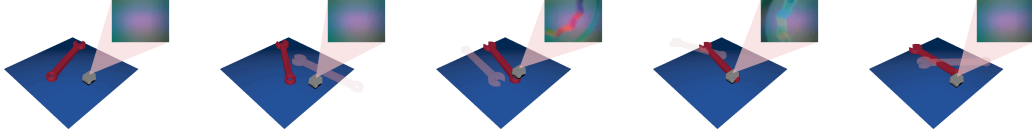


Figure 20: Agent trajectory in the Too1box environment. The agent collects local tactile readings of the wrench, sequentially integrating observations to regress its  $(x, y)$  position and orientation (represented as sine and cosine). The predicted pose is shown in transparent red in the simulation platform.

**TactileMNISTVolume:** In the TactileMNISTVolume environment (see Fig. 21), the agent must estimate the volume of a 3D handwritten-digit model using only tactile exploration. Pose perturbation causes small shifts during touch, so the agent must robustly follow the digit’s contour to accumulate sufficient surface samples for an accurate volume regression.

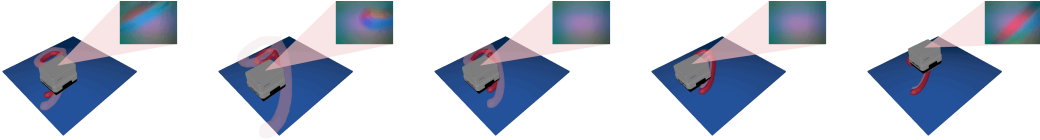


Figure 21: Agent trajectory in the TactileMNISTVolume environment. The sensor explores the digit surface under pose perturbations to regress the object’s normalized volume. We visualize here the predicted volume (transparent red) overlaid with the object mesh throughout the episode.

## G Extra Experiments

In this section, we present experimental results across all environments from both of our benchmark suites. We group the experiments based on similar evaluation metrics and apply our benchmark to active perception methods introduced in [52] and [8]. Specifically, TAP-SAC, TAP-CrossQ, TAP-RND, and TAP-PP0 refer to the Task-Agnostic Active Perception (TAP) framework proposed by [52]. TAP is a reinforcement learning (RL) framework that employs a transformer-based agent trained in a supervised setting. The variants SAC [61], PP0 [63], and CrossQ [62] denote the specific RL algorithms used within TAP. In contrast, RND represents a random exploration agent that uses TAP’s perception module but does not train the agent to propose actions. As another baseline, we evaluate HAM, the Haptic Attention Module proposed in [8]. HAM is a REINFORCE-based agent that does not incorporate a vision encoder. Therefore, we evaluate HAM only in environments that do not necessitate a vision encoder. Finally, we have also found that TAP-PP0 becomes unstable in combination with a vision encoder, so we only evaluated it on non-tactile environments as well.

**Classification environments** First, in Fig. 22 we present the results of the benchmarked methods on the classification environments from both `ap_gym` and TMBS, including those reported previously in Section 4 (with CircleSquare, TactileMNIST, and Starstruck repeated here for completeness). All classification results are evaluated using both average and final accuracy metrics. Overall, TAP-CrossQ and TAP-SAC demonstrate the strongest performance across the classification tasks, with TAP-CrossQ exhibiting slightly higher performance in general. In contrast, HAM and TAP-PP0 often struggle to outperform the random baseline TAP-RND in most environments where they were evaluated. A possible explanation for this could be the on-policy nature of these approaches, which does not allow for the reuse of samples for learning later on in the training. As expected, TAP-RND does not achieve a high performance in any of the environments, underlining the need for active perception.

To gain more insights into the behavior of policies during training, all environments log per-step metrics, which allows for an analysis of the predictions of the agent throughout individual episodes. Hence, the environments provide detailed protocols of the evaluation metrics over individual steps of an episode. As an example, see Fig. 23, which shows how the accuracy and correct label probability of the agents develop over the course of an episode of the TactileMNIST task.

Despite the comparatively strong performance of TAP-CrossQ and TAP-SAC, the challenges presented by the classification environments of this benchmark are far from being solved. Especially in the more complex environments, such as TinyImageNet with 200 classes and Starstruck with a challenging counting task, the performance exhibited by all approaches falls short of optimal. Both sample efficiency and final performance leave room for improvement, and new approaches are needed to close these optimality gaps and solve these tasks.

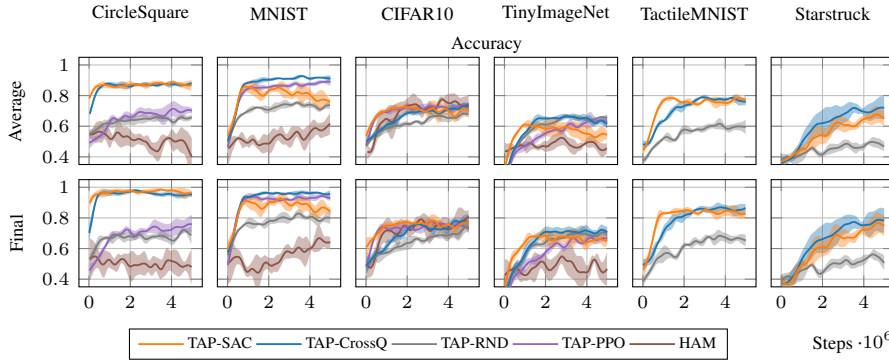


Figure 22: Average and final prediction accuracies for the baseline methods TAP-SAC, TAP-CrossQ, TAP-PP0, HAM [8], and a random baseline TAP-RND for the classification environments. All methods were trained on 5 seeds for 5M environment steps. Shaded areas represent one standard deviation. Metrics are computed on the evaluation variants of the tasks, except for Circle-Square, which has only two objects. For Starstruck, a correct classification requires predicting the exact number of stars.

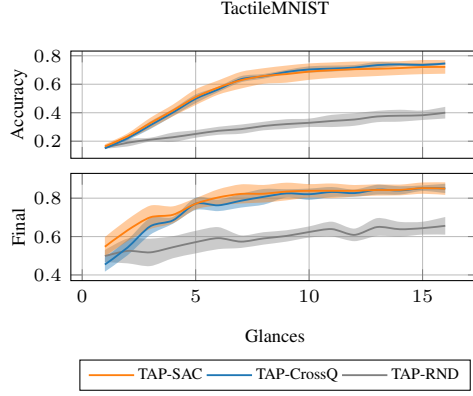


Figure 23: Exploration efficiency comparison of the final policies at the end of the training on the Tactile MNIST benchmark. Shown are the predicted probability of the correct label (left) and accuracy (right) after  $N$  tactile glances over the 16 steps until the episode terminates. The data is averaged over 5 seeds and smoothed over time steps within each seed.

**2D Localization environments** In our second set of experiments, we show the results for the localization environments, in which the agent has to estimate its 2D pose. These are depicted in Fig. 24. In general, the baseline methods seem to struggle more with this set of tasks than with the classification environments, with TAP-SAC even becoming unstable and crashing on the static LIDAR localization environments. These issues could be partly explained by the fact that none of the baseline methods was tuned on this type of task.

A surprising result is that HAM performs well on the LightDark environment, while TAP-SAC only barely outperforms the random baseline. Furthermore, the non-static LIDAR environments remain almost entirely unsolved, with neither method making substantial progress. The consistently low performance across these tasks is likely due to the substantial complexity and difficulty inherent in their design. In contrast to the static LIDAR environments, where agents can effectively memorize a fixed map, the non-static LIDAR environments present a novel map in each episode. As a result, solving these tasks requires the agent to generalize across maps by learning to associate its LIDAR observations with the corresponding bitmap representation provided as an additional input. This demands a level of perceptual and spatial reasoning that is inherently challenging — even for humans — which helps explain the limited success of current methods.

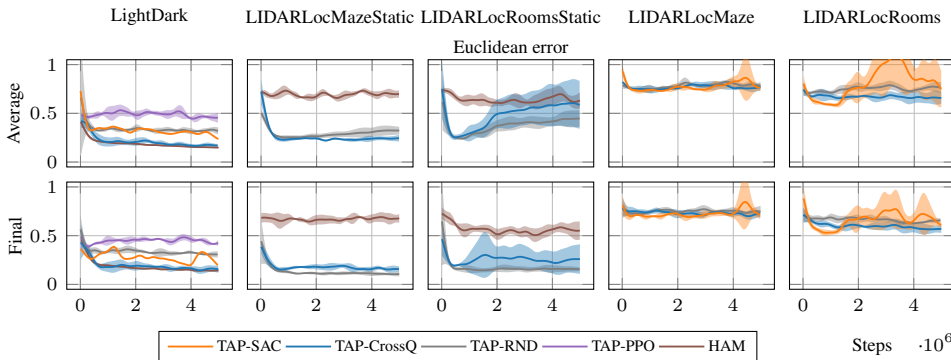


Figure 24: Average and final prediction errors for the baseline methods TAP-SAC, TAP-CrossQ, TAP-PPO, HAM [8], and a random baseline TAP-RND for the localization environments. All methods were trained on 5 seeds for 5M environment steps. Shaded areas represent one standard deviation. TAP-SAC and TAP-PPO became unstable on both static maze localization environments and crashed, which is why they are excluded from the respective plots. Note that LIDARLocMaze and LIDARLocRooms require a vision encoder and thus HAM and TAP-PPO cannot be evaluated on it.

**Image localization environments** Next, in Fig. 25, we show results from the image localization environments. These environments are particularly challenging and remain an open problem. In this setting, the agent receives only a small image glimpse and must actively explore a larger image to localize the target. Across these tasks, all agents exhibited comparable performance, with a slight downward trend in the Euclidean error over the course of training. TAP-CrossQ became unstable on TinyImageNetLoc, which is why it is excluded from the respective plots. We expect that the learning may be improved through targeted hyperparameter optimization specific to these environments.

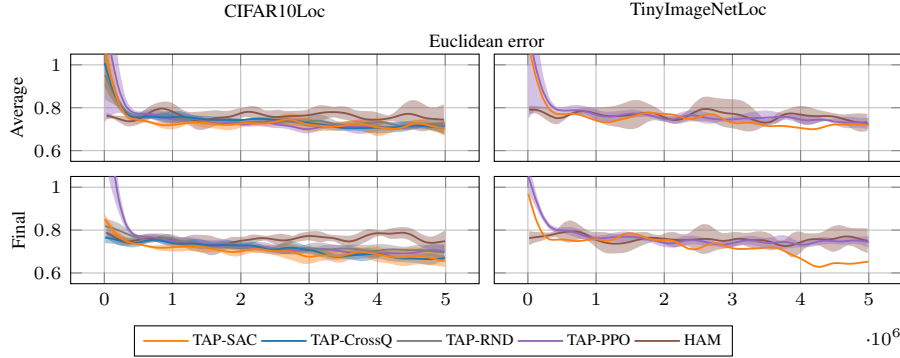


Figure 25: Average and final prediction accuracies for the baseline methods TAP-SAC, TAP-CrossQ, TAP-PPO, HAM [8], and a random baseline TAP-RND for the image localization environments. All methods were trained on 5 seeds for 5M environment steps. Shaded areas represent one standard deviation. TAP-CrossQ became unstable on the TinyImageNetLoc environment and crashed, which is why it is excluded from the respective plots. For TAP-SAC, only one out of 5 seeds on the TinyImageNetLoc task succeeded, while the others crashed due to learning instability. Hence, we show no standard deviation for this run.

**Pose estimation environments** For completeness, Fig. 26 shows a comparison of TAP-SAC, TAP-CrossQ, and TAP-RND on the pose estimation task within the Toolbox environment – reproducing the results presented in Section 4. In this evaluation, TAP-CrossQ achieves the lowest error across both the angular and linear components of the pose, indicating superior convergence performance compared to the other methods. Qualitatively, we see that only TAP-CrossQ seemed to have learned an effective exploration strategy of first moving the sensor in a circle to find the wrench and then moving towards one of the ends to determine the exact position and orientation. TAP-SAC did not learn an effective strategy and, thus, is on par with TAP-RND. Additionally, the variance across different seeds decreases notably throughout the training, meaning TAP-CrossQ consistently achieves low prediction errors.

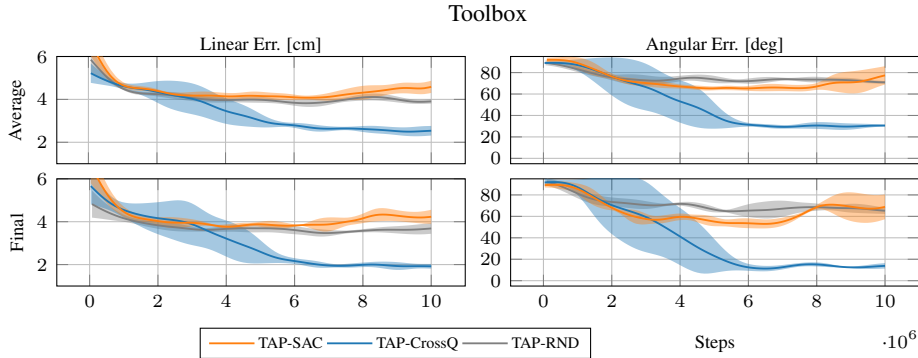


Figure 26: Average and final prediction errors for the baseline methods TAP-SAC, TAP-CrossQ, and a random baseline TAP-RND for the Toolbox environment. All methods were trained on 5 seeds for 10M environment steps. Shaded areas represent one standard deviation. We compute the linear and angular displacement between the prediction and the actual object pose as a metric.

**Volume estimation** Our final environment is TactileMNISTVolume, in which the agent must develop a strategy to estimate the volume of a digit. This task proved to be the most challenging

among the tasks of the TMBS environment. In this setting, TAP-CrossQ and TAP-SAC demonstrated similar performance. Notably, TAP-RND achieved comparable results in terms of final prediction accuracy, although it performed slightly worse on average throughout the training. This result can be attributed to the fact that within an episode TAP-SAC and TAP-CrossQ initially explore more efficiently than TAP-RND, but over time TAP-RND gathers enough information through random interaction to catch up. However, the overall error is still fairly high and may be improved via tuning on this environment.

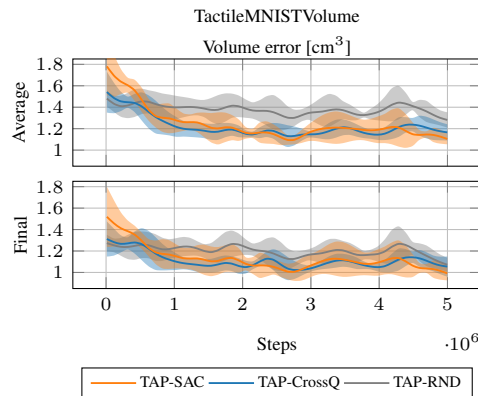


Figure 27: Average and final prediction accuracies for the baseline methods TAP-SAC, TAP-CrossQ, and a random baseline TAP-RND for the TactileMNISTVolume environment. All methods were trained on 5 seeds for 5M environment steps. Shaded areas represent one standard deviation. Metrics are computed on the evaluation variant of the tasks (TactileMNISTVolume-test), which contains objects unseen during training.

Table 17: Overview of the input modalities provided by the different environments. By *scalar input*, we mean real-valued vectors of arbitrary length. *Visual input* refers to image data represented by real-valued three-dimensional tensors of dimensions  $(W \times H \times C)$ , where  $W$  and  $H$  are width and height, respectively, and  $C$  is the number of channels. Some environments, such as CircleSquare or MNIST, provide the agent with only small glimpses of an image. Although these small glimpses are technically images, they are so small that it does not make sense to use a vision encoder to encode them. Hence, instead, we flatten them and process them as scalar data.

Suite	Environment	Task type	Scalar input	Vision input	$(W \times H \times C)$	Vision encoder
ap_gym	CircleSquare	Classification	✓	(✓)	$(5 \times 5 \times 1)$	✗
	MNIST	Classification	✓	(✓)	$(5 \times 5 \times 1)$	✗
	CIFAR10	Classification	✓	(✓)	$(5 \times 5 \times 3)$	✗
	TinyImageNet	Classification	✓	(✓)	$(10 \times 10 \times 3)$	✗
	CIFAR10Loc	Regression	✓	(✓)	$(5 \times 5 \times 3)$	✗
	TinyImageNetLoc	Regression	✓	(✓)	$(10 \times 10 \times 3)$	✗
	LightDark	Regression	✓	✗		✗
	LIDARLocMazeStatic	Regression	✓	✗		✗
	LIDARLocRoomsStatic	Regression	✓	✗		✗
	LIDARLocMaze	Regression	✓	✓	$(21 \times 21 \times 1)$	✓
	LIDARLocRooms	Regression	✓	✓	$(32 \times 32 \times 1)$	✓
TMBS	TactileMNIST	Classification	✓	✓	$(64 \times 64 \times 3)$	✓
	TactileMNISTVolume	Regression	✓	✓	$(64 \times 64 \times 3)$	✓
	Toolbox	Regression	✓	✓	$(64 \times 64 \times 3)$	✓
	Starstruck	Classification	✓	✓	$(64 \times 64 \times 3)$	✓

## H Implementation Details

The implementation of TAP, TAP-PP0, and HAM used in the experiments of this work is based on JAX [56] and the Flax deep-learning framework [66], and uses the Hugging Face transformer implementations [67]. For performance reasons, the entire training loop is JIT-compiled, and all interaction with the environment happens through host callbacks. This scheme ensures maximal performance at the cost of limiting flexibility in the implementation.

A bottleneck in many deep-learning applications is the transfer of data between VRAM (GPU) and RAM (CPU). To mitigate this bottleneck as much as possible, we store the replay buffer in the VRAM, which limits the interactions between the GPU and the CPU to stepping the environment and logging data. However, typically, there is less VRAM than RAM present, which limits the size of the replay buffer in case of environments with vision input. We found that our Nvidia RTX A5000 GPUs with 24GB of VRAM can hold around 3M transitions in the replay buffer before running out of space if we scale visual inputs to  $32 \times 32$ px. Hence, for the vision-encoder configurations, we use a replay buffer size of 3M, while for the non-vision-encoder configurations, we use a replay buffer size equal to the total number of environment steps. An overview of which environments require vision encoders is given in Table 17.

All our experiments were conducted on Nvidia RTX A5000 or RTX 3090 GPUs with the hyperparameters defined in Table 3. For vision-encoder configurations, we fully allocate one GPU for each run. Depending on the algorithm, a run of  $5M$  steps takes around 40-50 hours.

Since non-vision-encoder configurations do not require much VRAM, we run multiple runs on the same GPU to use resources more efficiently. Depending on the environment and algorithm, the data of up to 28 parallel runs fits into the VRAM of a single RTX A5000/3090 GPU. Hence, the runtime of these runs varies greatly with the number of runs per GPU and is, thus, not meaningful to report. However, we found that HAM and PP0 runs are generally about four times as fast as TAP runs.

## Appendix References

- [68] Alexander I Cowen-Rivers, Wenlong Lyu, Rasul Tutunov, Zhi Wang, Antoine Grosnit, Ryan Rhys Griffiths, Alexandre Max Maraval, Hao Jianye, Jun Wang, Jan Peters, et al. Hebo: Pushing the limits of sample-efficient hyper-parameter optimisation. *Journal of Artificial Intelligence Research*, 74:1269–1349, 2022.
- [69] Alex Church, John Lloyd, Raia Hadsell, and Nathan F. Lepora. Tactile sim-to-real policy transfer via real-to-sim image translation. In Aleksandra Faust, David Hsu, and Gerhard Neumann, editors, *Proceedings of the 5th Conference on Robot Learning*, volume 164 of *Proceedings of Machine Learning Research*. PMLR, 08–11 Nov 2022.
- [70] Yijiong Lin, John Lloyd, Alex Church, and Nathan F Lepora. Tactile gym 2.0: Sim-to-real deep reinforcement learning for comparing low-cost high-resolution robot touch. *IEEE Robotics and Automation Letters*, 7(4):10754–10761, 2022.
- [71] Phillip Isola, Jun-Yan Zhu, Tinghui Zhou, and Alexei A Efros. Image-to-image translation with conditional adversarial networks. In *Computer Vision and Pattern Recognition (CVPR), 2017 IEEE Conference on*, 2017.